Novel Redox Active Vanadium(V)-Dithiolene Complexes for Efficient Supercapacitive Energy Storage: Role of Selenium Functionalization on Pseudo-capacitive Properties

Sangita Mondal,[a] T Kedara Shivasharma,[b] Sujit Das,[a] Mayur Thosare,[b] Christel Livia Mascarenhas,[a] Babasaheb R. Sankapal*,[b] Kartik Chandra Mondal*[a]

[a]*Department of Chemistry, Indian Institute of Technology Madras, Chennai, 600036, Tamil Nadu, India*

[b]*Nano Materials and Device Laboratory, Department of Physics, Visvesvaraya National Institute of Technology, South Ambazari Road, Nagpur-440010 (M.S.) India.*

Supporting Information

Table S1: Comparative data for reported vanadium based supercapacitor materials and the two newly synthesized V(V)-dithiolene complexes

Material	Nature	Substrate	Electrolyte	Potential Window (V)	Specific capacitance ($F \cdot g^{-1}$)	Stability	Ref.
$V_2O_5/VACNTs$	Inorganic	Ni Foam	1 M Na_2SO_4	1.1 V	284 @ 2 A $\cdot g^{-1}$	89.3 % @ 2500	[S1]
$Sn-V_2O_5/rGO$	Inorganic	Ni Plate	1 M Na_2SO_4	0.9 V	159.37 @ 1 $A \cdot g^{-1}$	95 % @ 1000	[S2]
V_2O_5	Inorganic	Ni Foam	1 M Na_2SO_4	1.0 V	235 @ 1 $A \cdot g^{-1}$	---	[S3]
$Mo-V_2O_5$	Inorganic	Ni	1 M KCl	0.8 V	175 $mF \cdot cm^{-2}$ @ 1 $mA \cdot cm^{-2}$	---	[S4]
$Ni-V_2O_5$	Inorganic	---	1 M Na_2SO_4	2.5 V	152 @ 10 $mV \cdot s^{-1}$	---	[S5]
rGO/V_2O_5	Inorganic	Carbon Fabric	1 M H_2SO_4	1.2 V	120 @ 2 $A \cdot g^{-1}$	100 % @ 5000	[S6]
$TNT-VO_2$	Inorganic	Ti Foil	1 M KCl	0.8 V	152.21 @ 5 $mV \cdot s^{-1}$	99 % @ 3000	[S7]
$W-VO_2$	Inorganic	Ni Foil	1 M Na_2SO_4	0.7 V	253 @ 1 $A \cdot g^{-1}$	---	[S8]
VO_2-MXene	Inorganic	Graphite Sheet	1 M Na_2SO_4	1.8 V (Liquid Device)	286 @ 2 $A \cdot g^{-1}$	97 % @ 10000	[S9]
VO_x. Ti-VACNT	Inorganic	Ni Disk	1 M Na_2SO_4	1.8 V	313 @ 2 $mV \cdot s^{-1}$	@400	[S10]
1T-VS_2/MXene	Inorganic	Ni Foam	0.5 M K_2SO_4	1.0 V	106.38 @ 0.2 $A \cdot g^{-1}$	---	[S11]
MXene-V_2O_5	Inorganic	Stainless steel mesh	1 M H_2SO_4	0.5 V	169.7 @ 10 $A \cdot g^{-1}$	---	[S12]
Complex **1**	Inorganic Complex	Stainless steel	1 M Na_2SO_4	0.8 V	82.82 @ 5 $mV \cdot s^{-1}$ 38.02 @ 0.2 $mA \cdot cm^{-2}$	63.13 % @ 2000	This work
Complex **2**	Inorganic Complex	Stainless steel	1 M $LiClO_4$	0.85 V	76.56 @ 5 $mV \cdot s^{-1}$ 21.90 @ 0.6 $mA \cdot cm^{-2}$	104.39 % @ 2000	This work

S1. Synthesis of Se-functionalized anionic dithioleen radical ligand

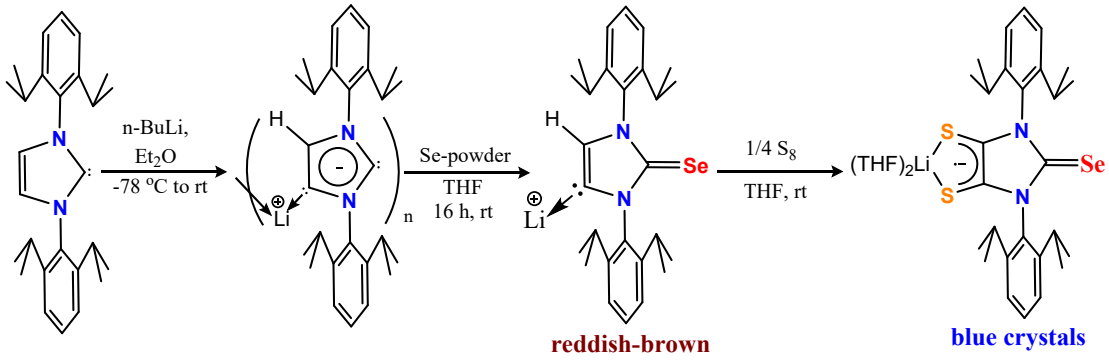

Procedure:

This ligand was synthesized following the similar procedure reported by Robinson et al. (see reference 22. in main manuscript) with a slight modification in the second step using three equivalents of selenium instead of Sulfur.

In a 100 mL Schlenk flask, N-heterocyclic carbene (5 g, 12.85 mmol) was dissolved in dry THF under argon atmosphere. Three equivalent of selenium powder (3.05 g, 38.55 mmol) was added into it, resulting in a reddish-brown solution. Sulfur powder (0.825 g, 25.7 mmol) was then added, leading to a deep blue solution, indicating the formation of the 2-seleno dithiolene radical complex. The dark blue crystals were isolated from a THF/hexane mixture. Yield: 80%.UV-vis-NIR band (nm): 326, 480 and 961. Elemental analysis (C, H, N) (Calc.) (%): C, 61.63 (61.75); H, 7.31 (7.40); N, 4.02 (4.11).

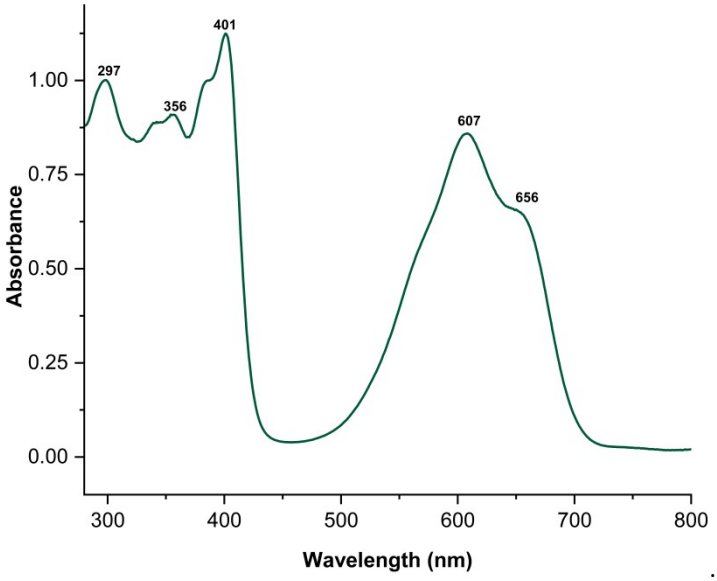

UV-Visible spectrum of ligand $[Li(THF)_4][V(SS\text{-}NHC{=}Se)_3]$ in THF

S2. Thermogravimetric analysis plot

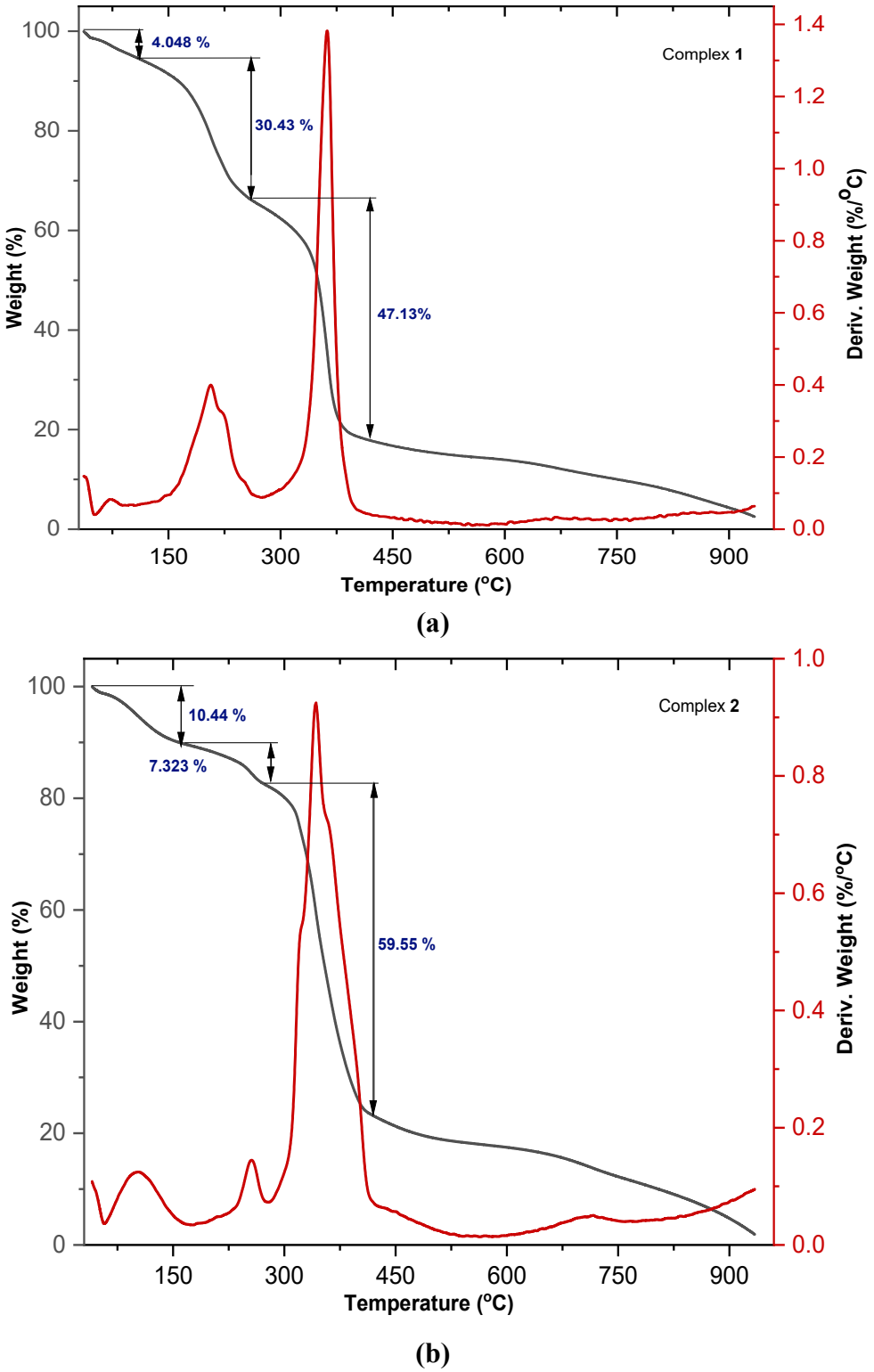

Figure S1. Thermogravimetric analysis (TGA) plots of complexes (a) **1** and (b) **2.**

S3. Theoretical Calculations

The geometry optimization of the complexes $[Li(THF)_4][V(SS\text{-}NHC{=}S)_3]$ (**1**) and $[Li(THF)_4][V(SS\text{-}NHC{=}Se)_3]$ (**2**) were carried out at the BP86[S13]-D3(BJ)[S14, S15]]/Def2-TZVPP [S16] level of theory by replacing Dip groups with Me as **1'** and **2'** in singlet monoanion state in both the gaseous phase (**1a'** and **2a'**) as well as in solvent medium (THF) (**1b'** and **2b'**) and dianion electronic state in gaseous phase [$(\mathbf{1'})^{\bullet-}$ and $(\mathbf{2'})^{\bullet-}$] with the help of DFT using the Gaussian 16 package[S17]. The geometry optimization for the singlet monoanion is favoured by minima on the potential energy surface, followed by no negative frequency. The energy difference between singlet monoanion and doublet dianion in gas phase lies between 5.326-10.318 kcal/mol. The NBO 6.0 program[S18] is used to perform the NBO calculations[S19] of the complexes, mulliken charges, mulliken spin densities and natural bond orbitals for both electronic states to understand their electronic structures. The doublet dianion state was further studied to investigate its accessibility in the electrochemical process .

Table S2: The vanadium - dithiolene complexes in their total charge and spin multiplicity used for optimisation at the BP86-D3(BJ)/def2tzvpp level of theory using DFT.

Complexes	Total Charge (q)	Spin Multiplicity (2S+1)
V^{5+} (**1a'**)	-1	1 (S = 0)
V^{5+} (**1b'**)	-1	1 (S = 0)
V^{4+} (**1c'**)	-2	2 (S = 1/2)
V^{5+} (**2a'**)	-1	1 (S = 0)
V^{5+} (**2b'**)	-1	1 (S = 0)
V^{4+} (**2c'**)	-2	2 (S = 1/2)

Table S3: The HOMO-LUMO energy difference of the complexes in the gas phase and THF as a solvent medium at the BP86/def2tzvpp level of theory.

Complexes	HOMO-LUMO energy gap in the gas phase (eV)	HOMO-LUMO energy gap in the THF medium (eV)
V^{5+} (**1'**)	1.186 (**1a'**)	1.159 (**1b'**)

V^{5+} (**2'**)	1.122 (**2a'**)	1.154 (**2b'**)
V^{4+} (**1'**)	0.419 (**1c'**)	----------
V^{4+} (**2'**)	0.432 (**2c'**)	----------

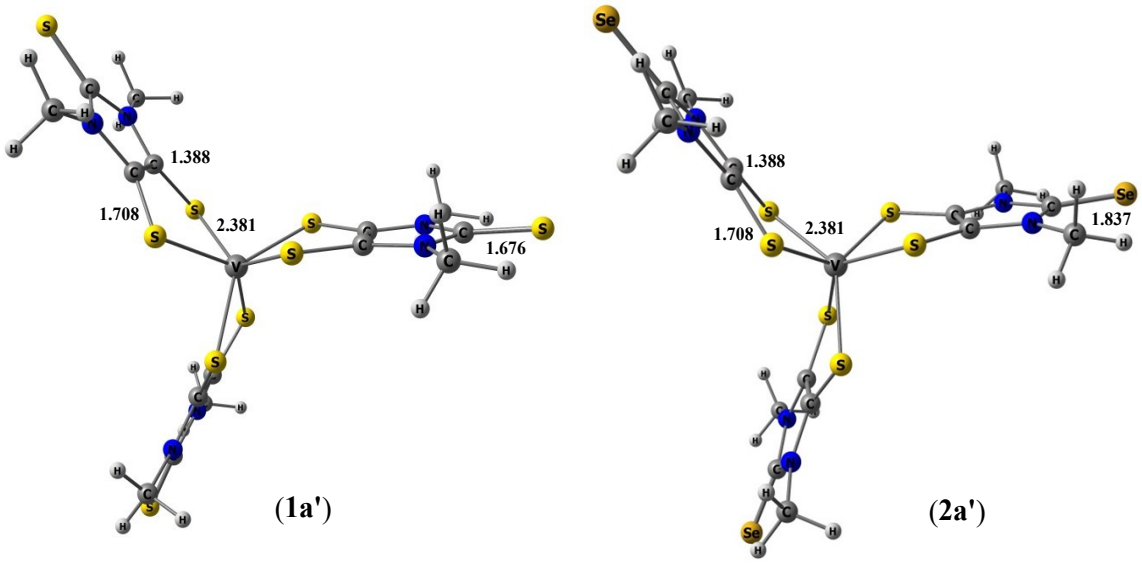

Figure S2. Optimised geometries of complexes **1'** and **2'** in gas phase at the BP86-D3(BJ)/def2tzvpp level of theory for singlet monoanion state. Bond lengths are in Å.

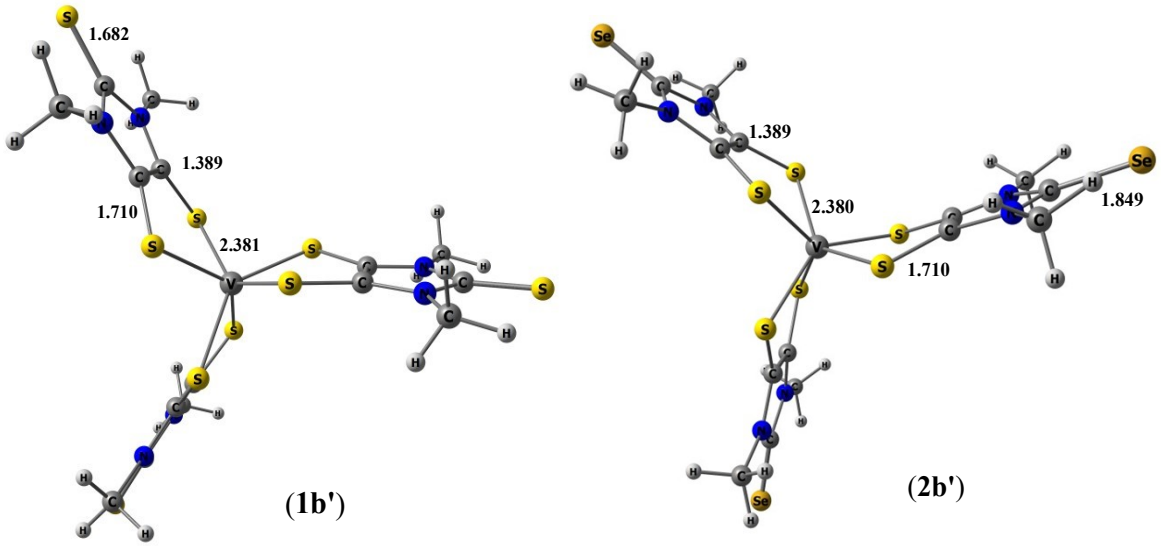

Figure S3. Optimised geometries of complexes **1'** and **2'** in solvent (THF) at the BP86-D3(BJ)/def2tzvpp level of theory for singlet monoanion state. Bond lengths are in Å.

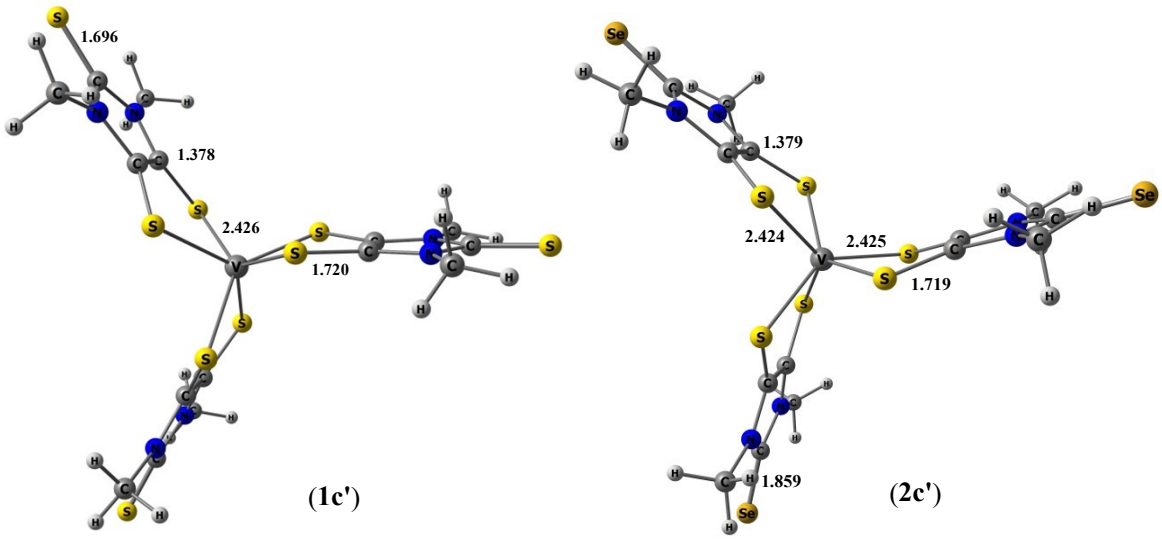

Figure S4. Optimised geometries of complexes **1'** and **2'** in gas phase at the BP86/def2tzvpp level of theory for doublet dianion state. Bond lengths are in Å.

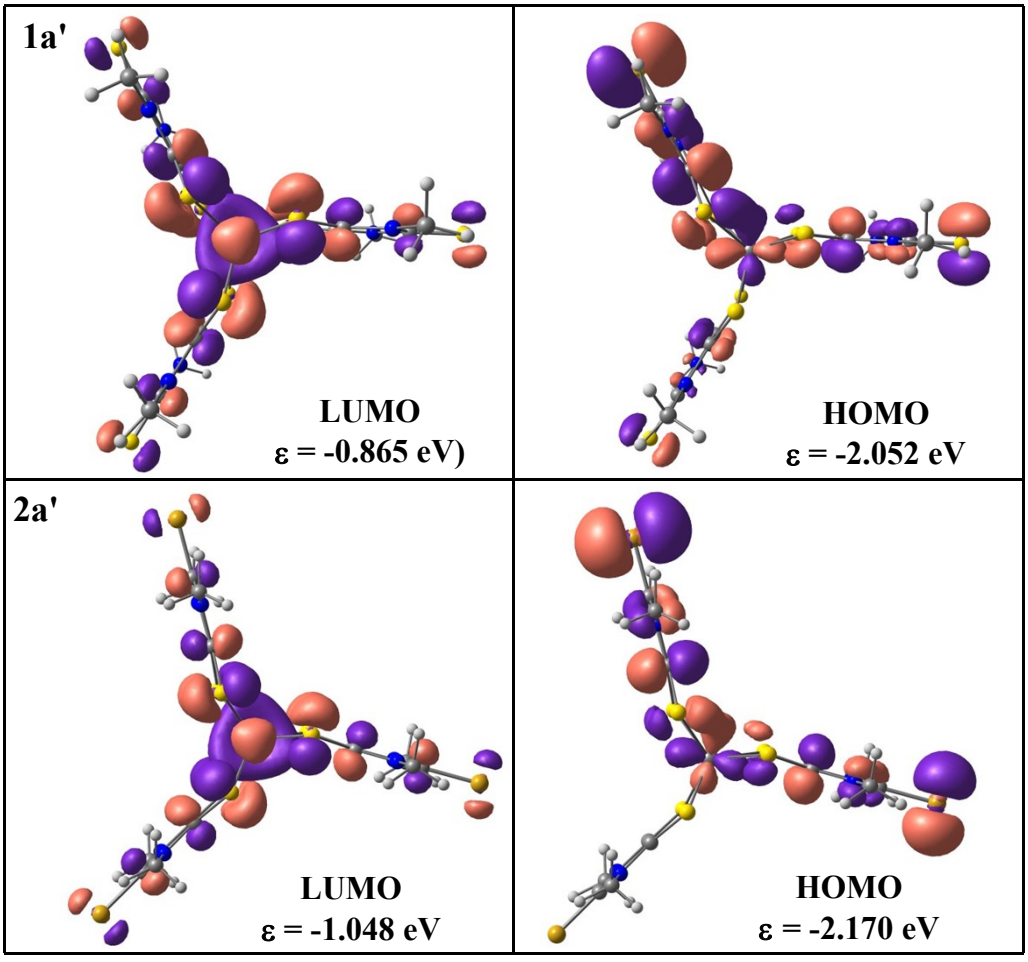

Figure S5. NBO figures of complexes **1'** and **2'** in singlet monoanion state at gaseous phase at the BP86-D3(BJ)/def2tzvpp level of theory.

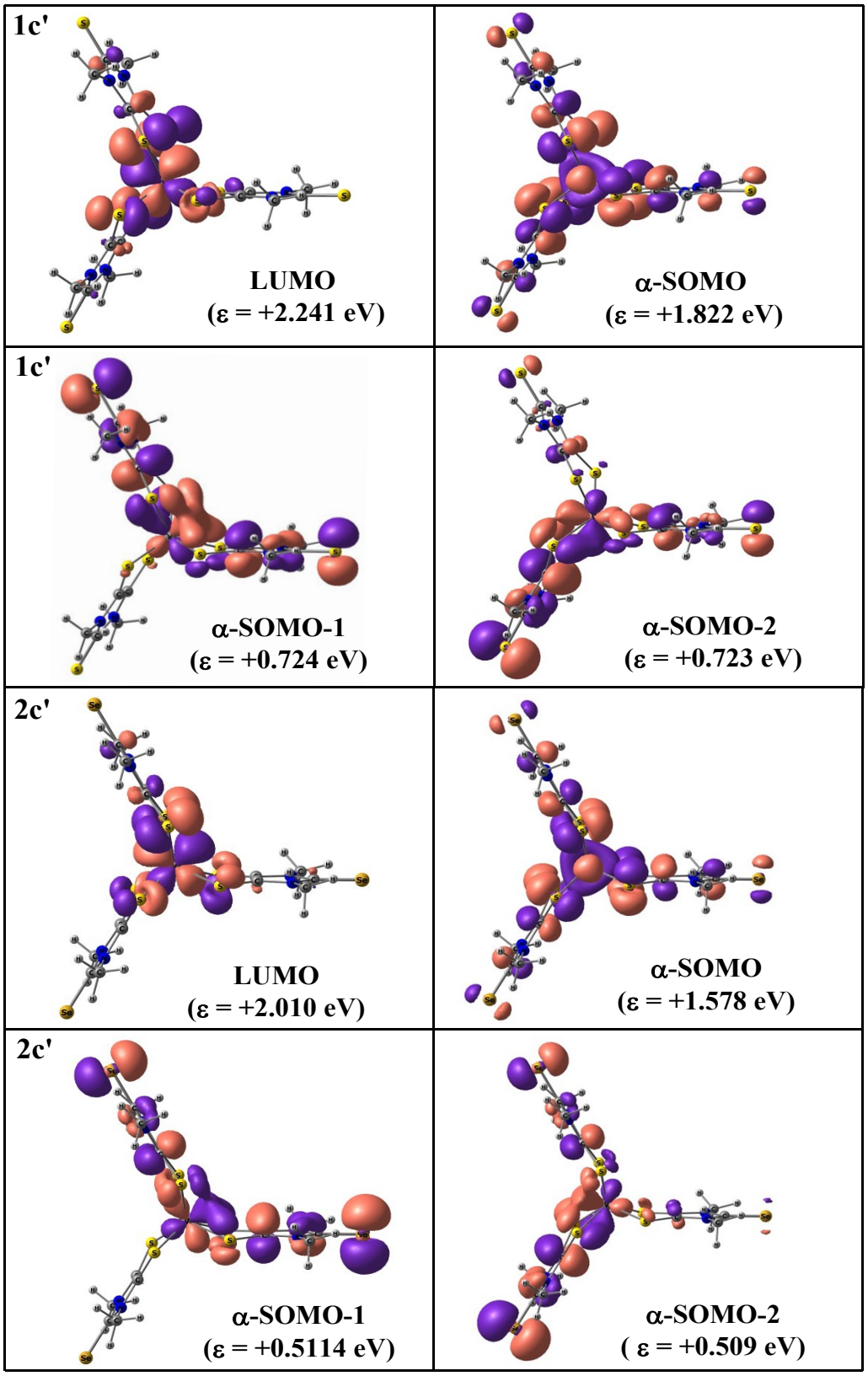

Figure S6. NBO figures of complexes **1'** and **2'** in doublet dianion state at gaseous phase at the BP86-D3(BJ)/def2tzvpp level of theory.

S4. Packing arrangements

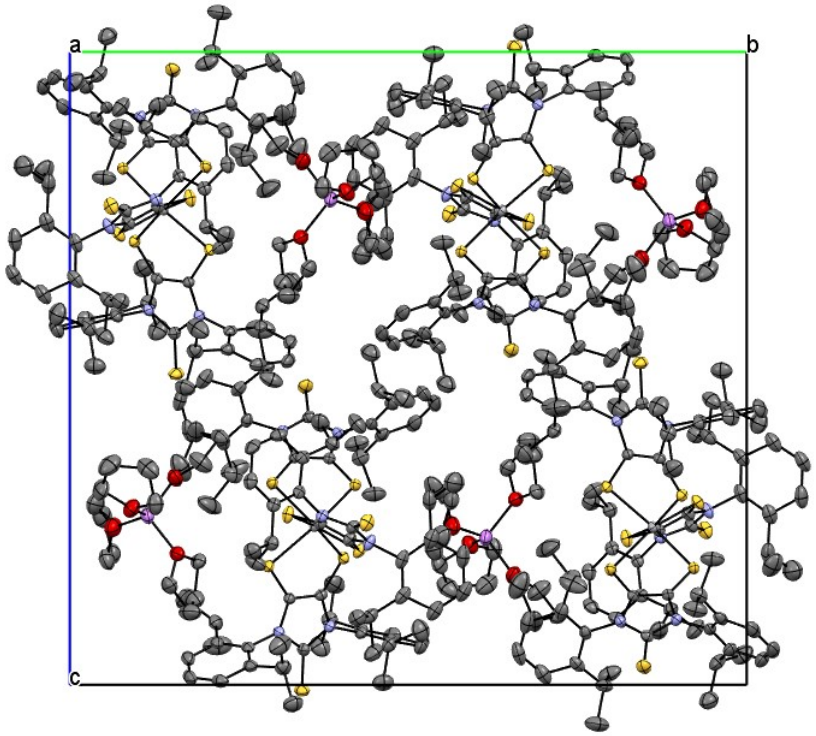

(a)

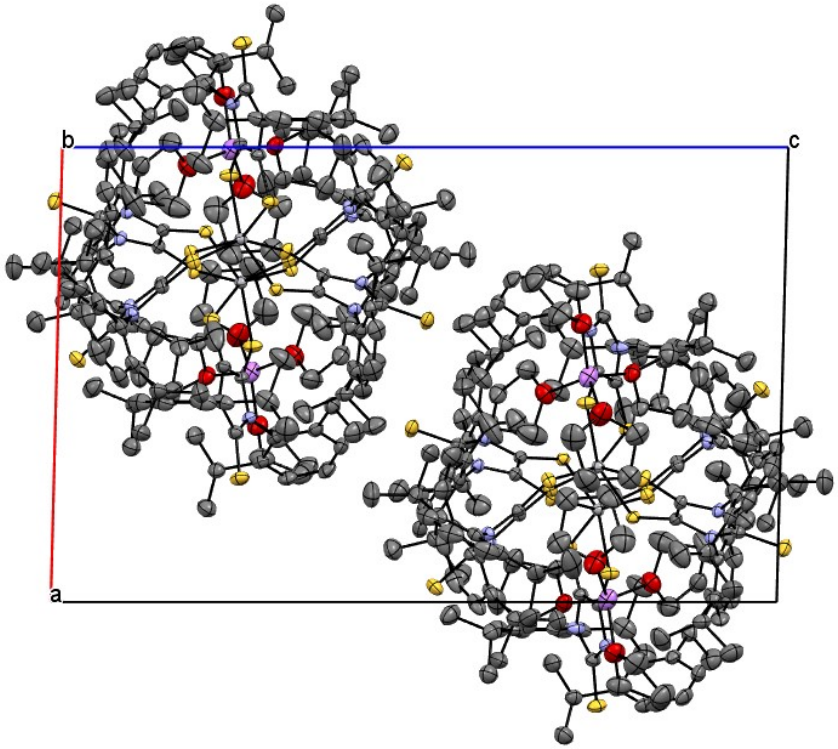

(b)

Figure S7. Crystal packing arrangement for complex **1**; **(a)** along a-axis, **(b)** along b-axis.

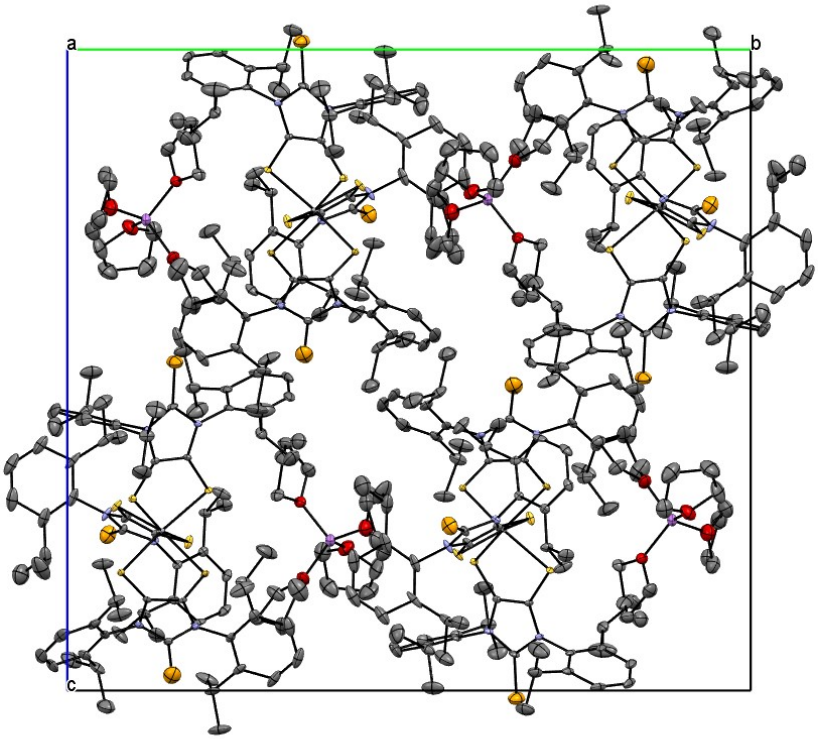

(a)

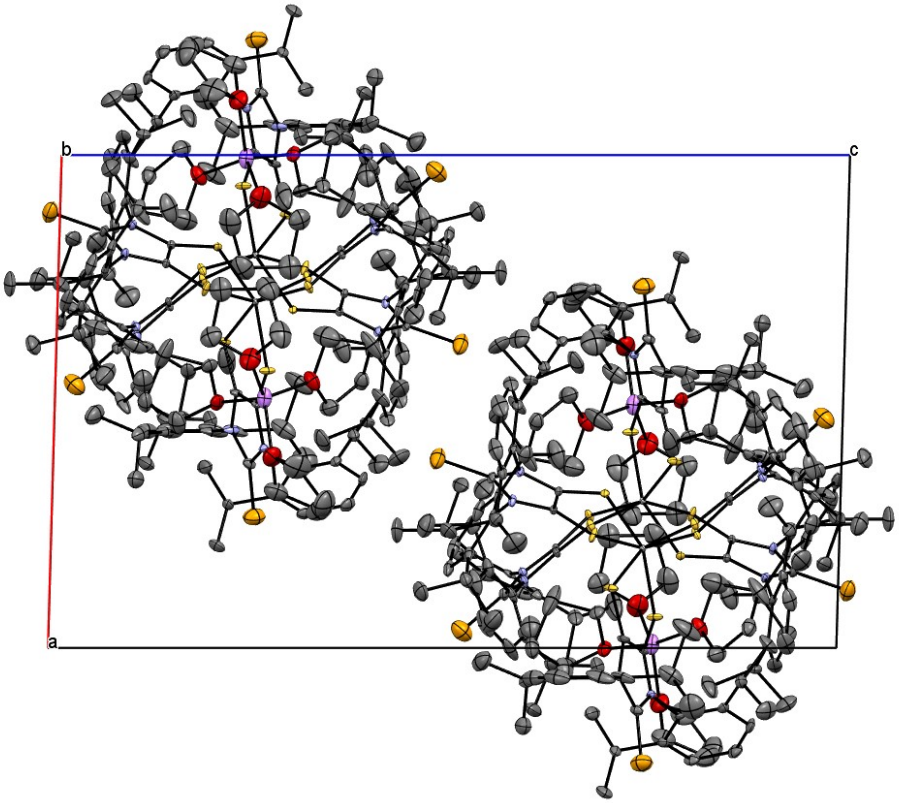

(b)

Figure S8. Crystal packing arrangement for complex **2**; **(a)** along a-axis, **(b)** along b-axis.

S5. Infrared spectroscopy

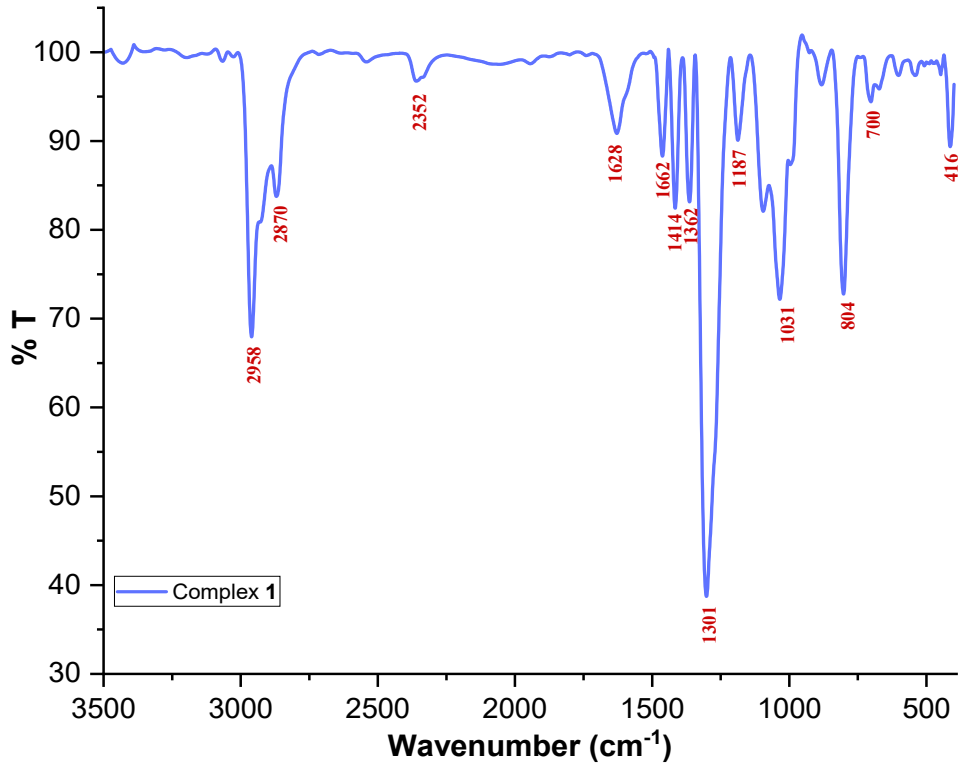

(a)

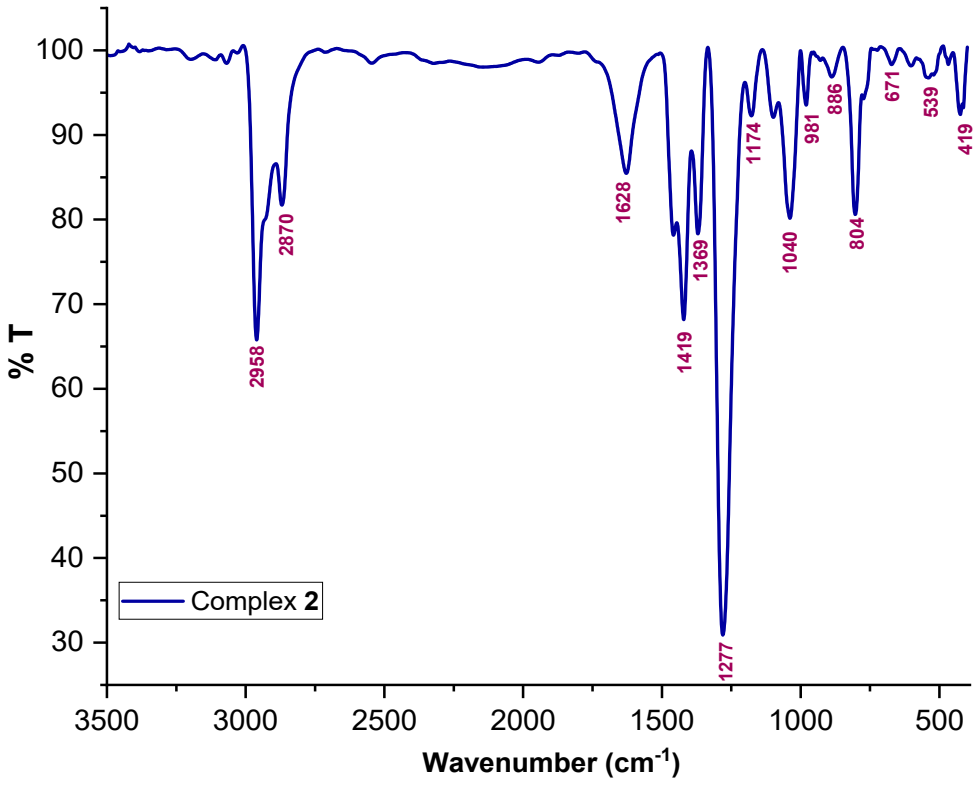

(b)

Figure S9. Infrared spectra of complexes (a) **1'** and (b) **2'** in KBr pellet.

S6. Electron paramagnetic resonance spectroscopy

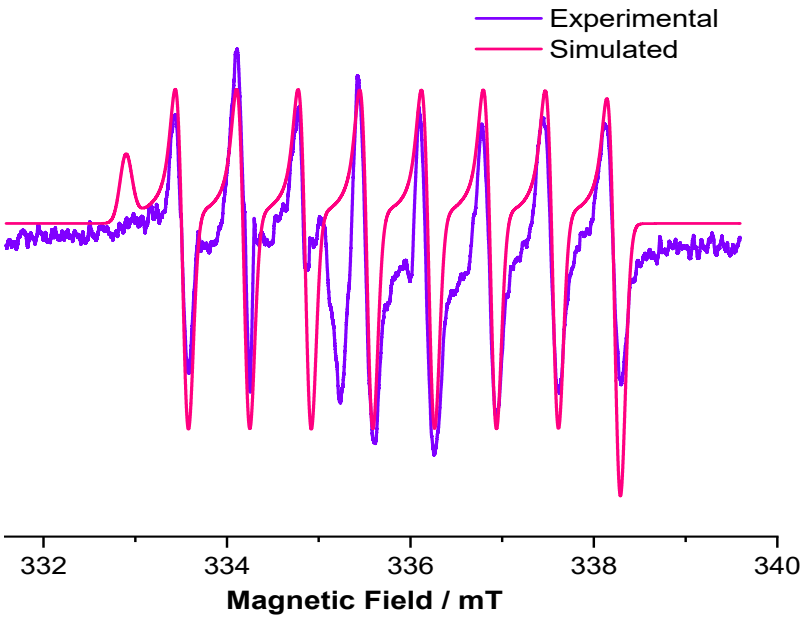

Figure S10. X-band EPR spectra of complex $\mathbf{1}^{\bullet-}$ at 293 K in THF. Blue and red lines represent the experimental and simulated spectra using EasySpin program. Zoomed-in spectra. Simulation parameters: $g_{\parallel}$ = 2.01352, $g_{\perp}$ = 2.00962,, LW1 = 0.128459 mT, LW2 = 0.001 mT, A(V) = 18.9304 MHz, Centre of frequency 335.7 mT.

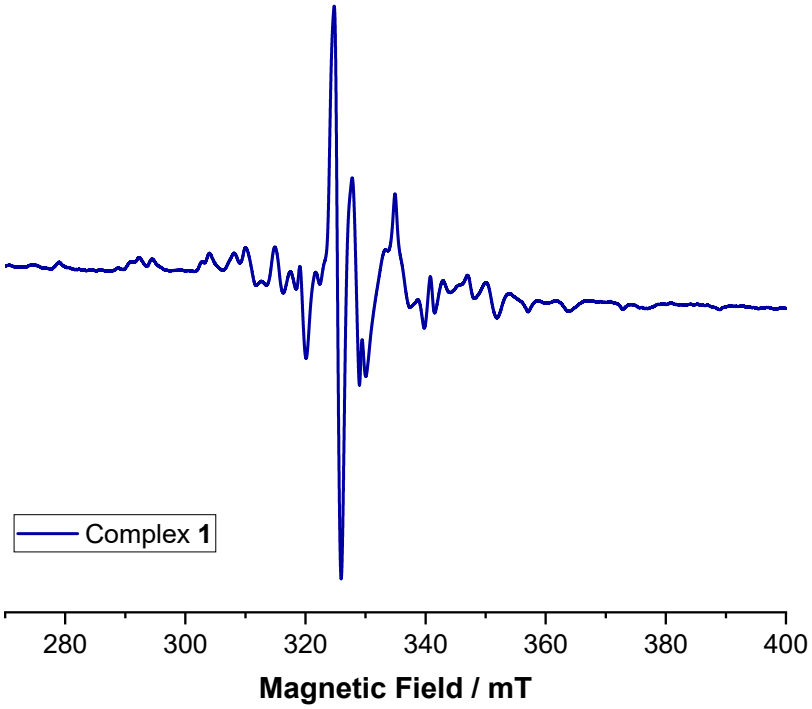

Figure S11. X-band EPR spectra of complex $\mathbf{1}^{\bullet-}$ at 90 K in THF.

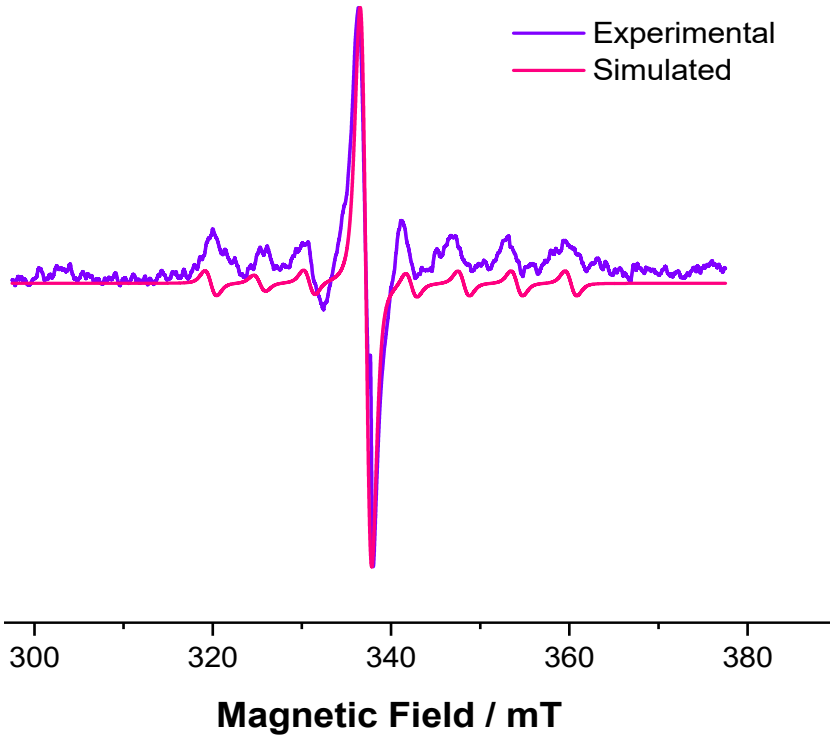

Figure S12. X-band EPR spectra of complex $\mathbf{2}^{\bullet-}$ at 298 K in THF. Blue and red lines represent the experimental and simulated spectra using EasySpin program. Simulation parameters:g(Radical unpaired e^-) = 2.00223, g(Metal unpaired e^-) = 1.98486, LW1 = 0.965454 mT, LW2 = 0.523409 mT, A(^{51}V) = 160.284MHz, Centre of frequency 337.1 mT.

S7. UV-vis-NIR spectroscopy

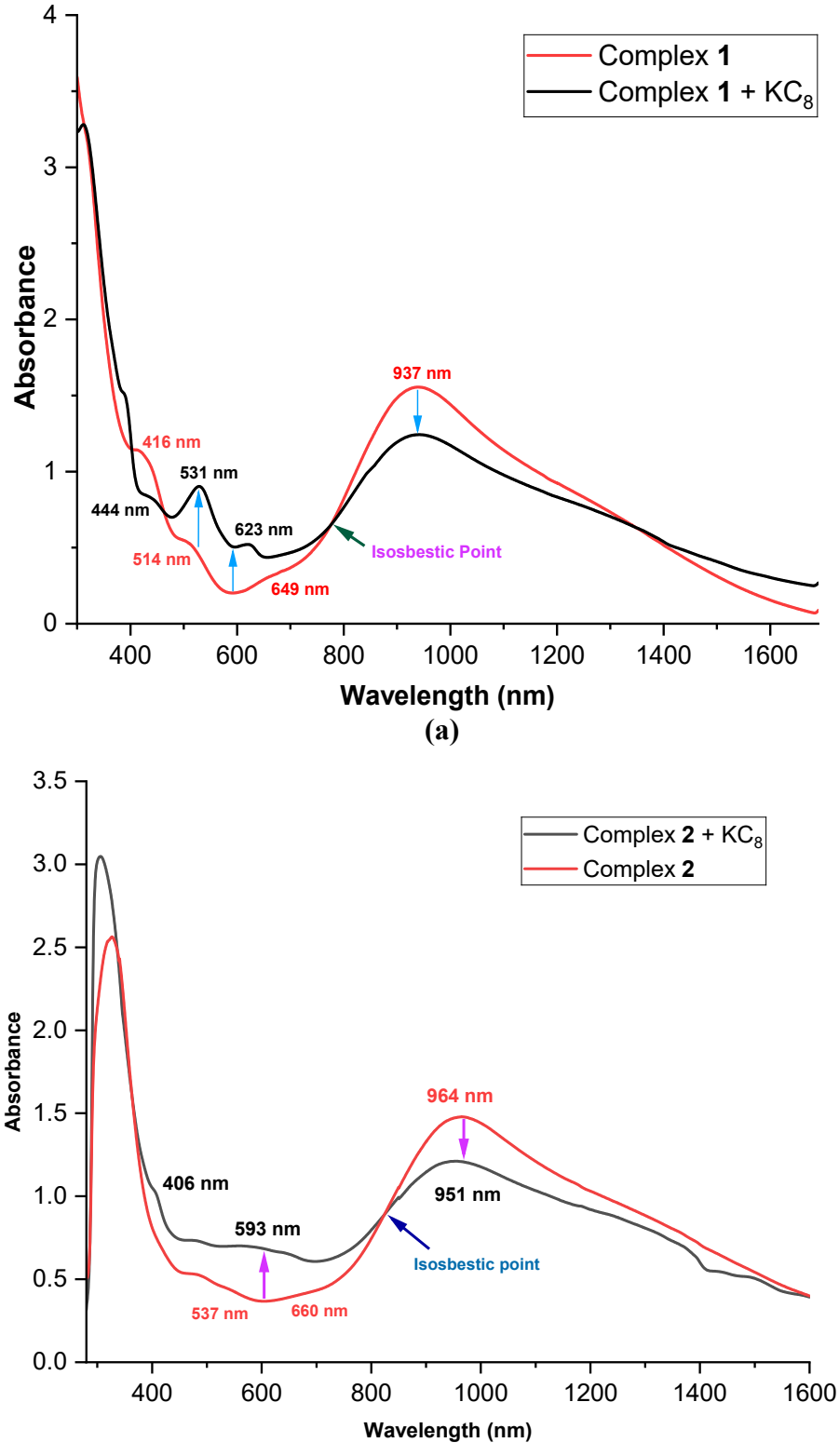

Figure S13. UV-vis-NIR spectra comparision after reduction with KC_8 (black line). **(a)** Complex **1**, **(b)** complex **2**.

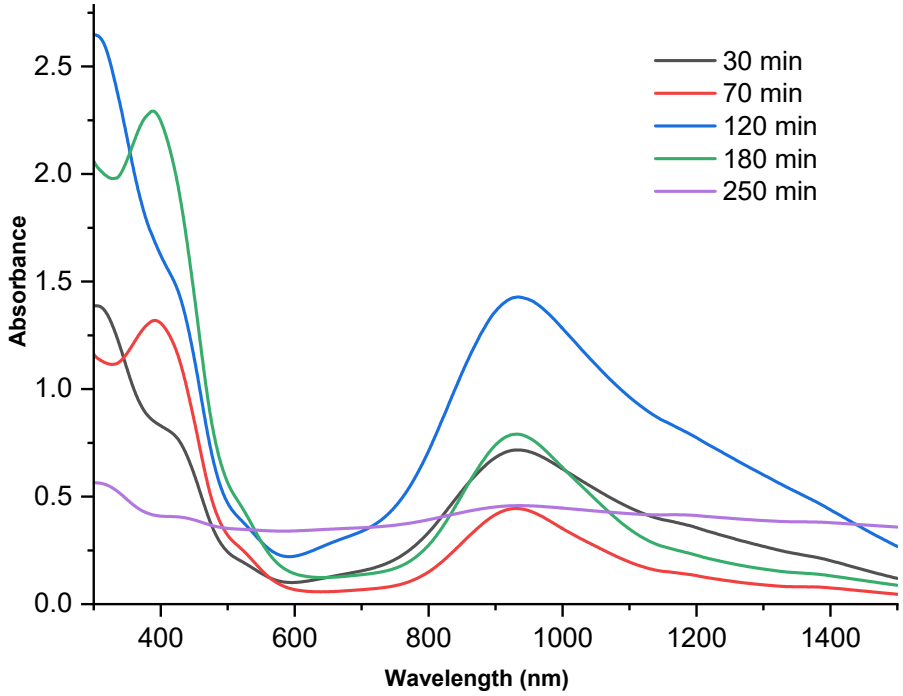

Figure S14. Time dependent UV-vis-NIR absorption spectra for complex **1** at 30, 70, 120, 180, and 250 min of intervals respectively.

S8. TD-DFT calculations at BP86-D3(BJ)/def2tzvpp level of theory:

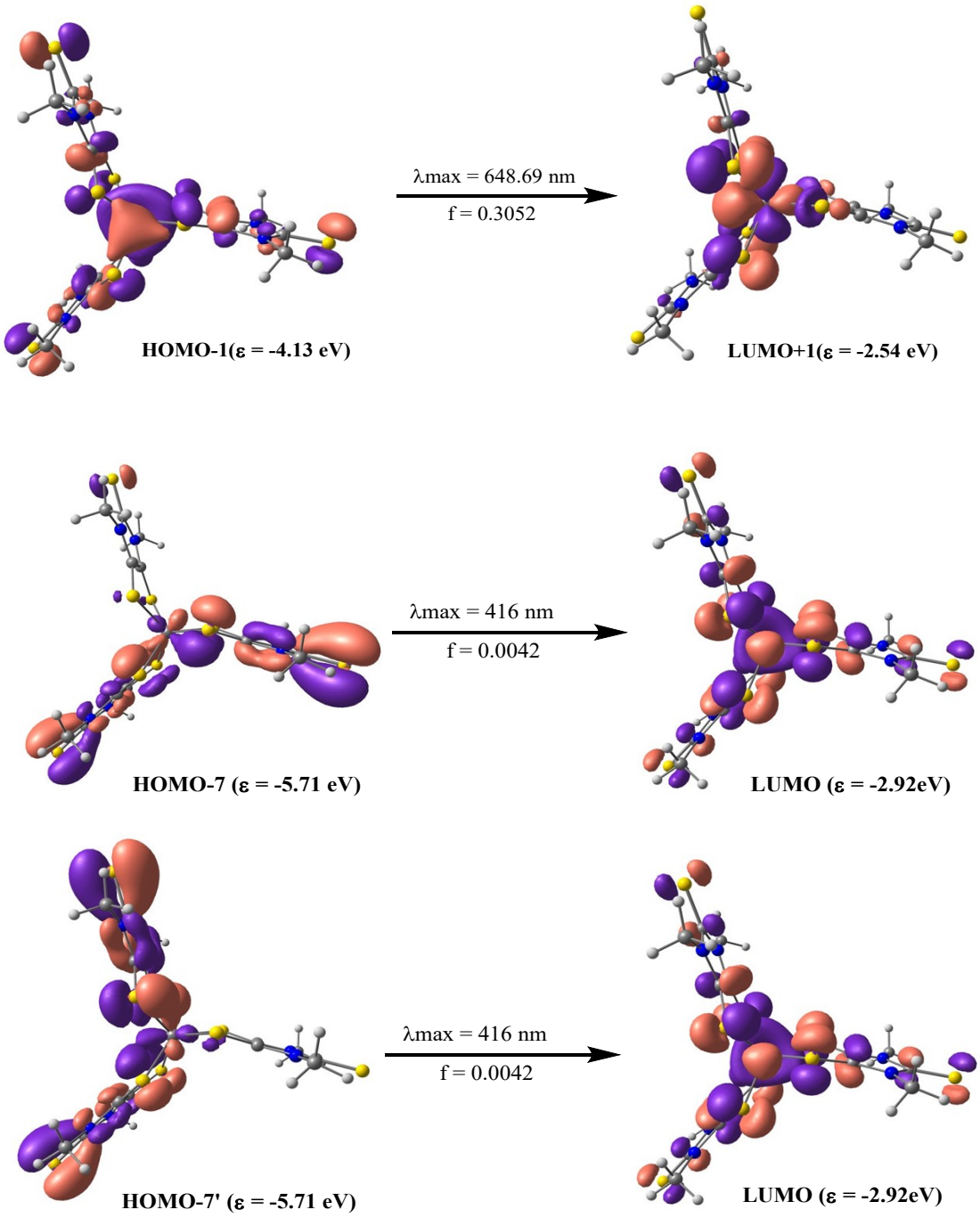

Figure S15. TD-DFT results of complex **1**.

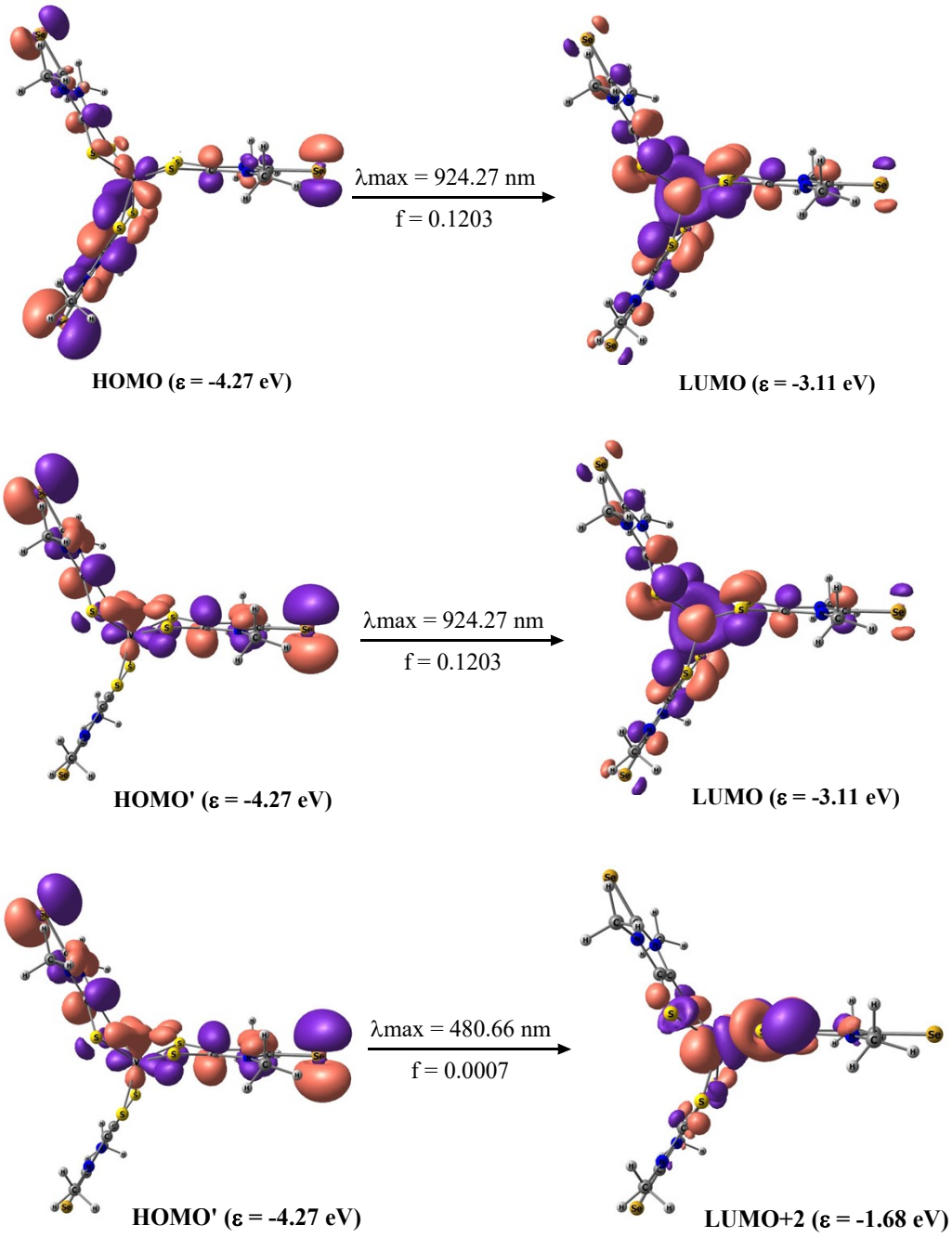

Figure S16. TD-DFT results of complex **2**.

S9. NMR Spectroscopy

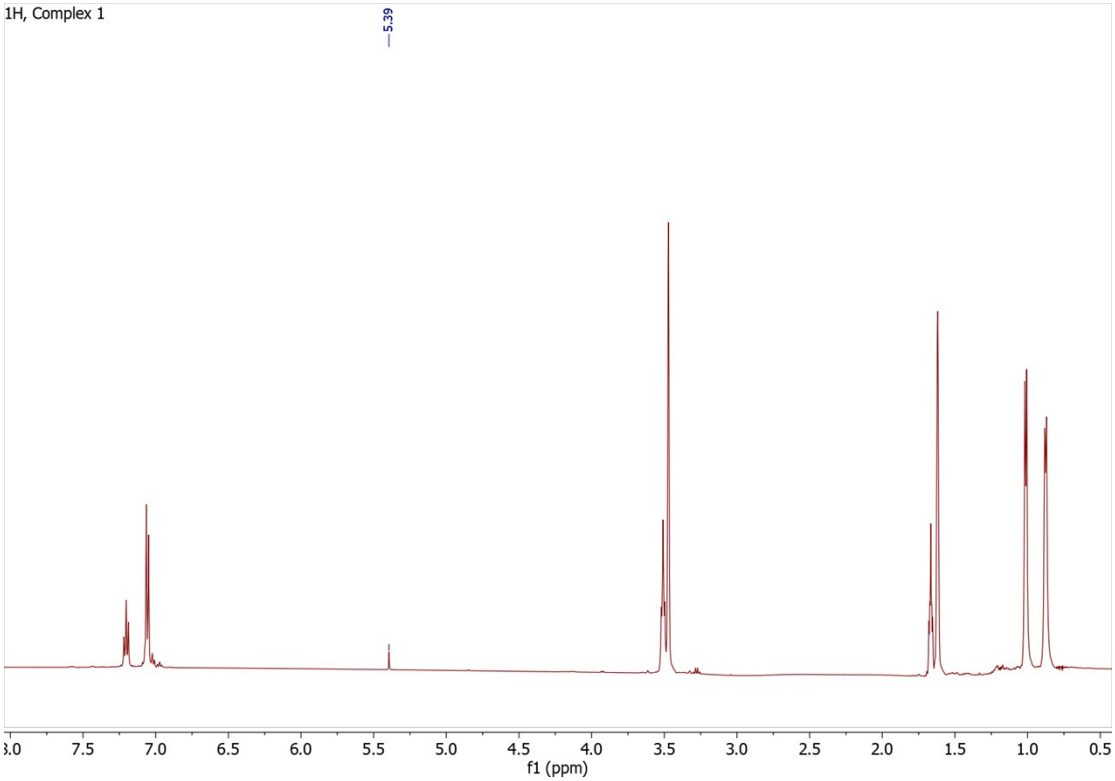

Figure S17. ^{1}H NMR spectrum of complex **1** in THF-d_8 at RT (1024 scans)

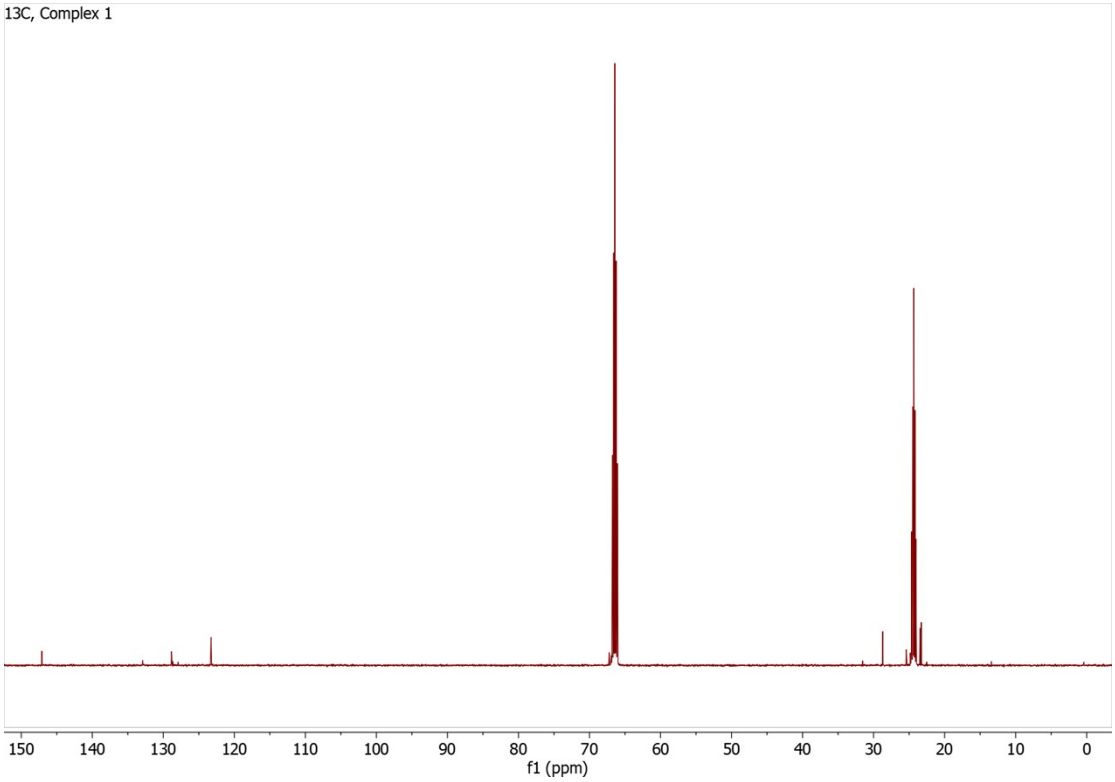

Figure S18. ^{13}C NMR spectrum of complex **1** in THF-d_8 at RT (1024 scans)

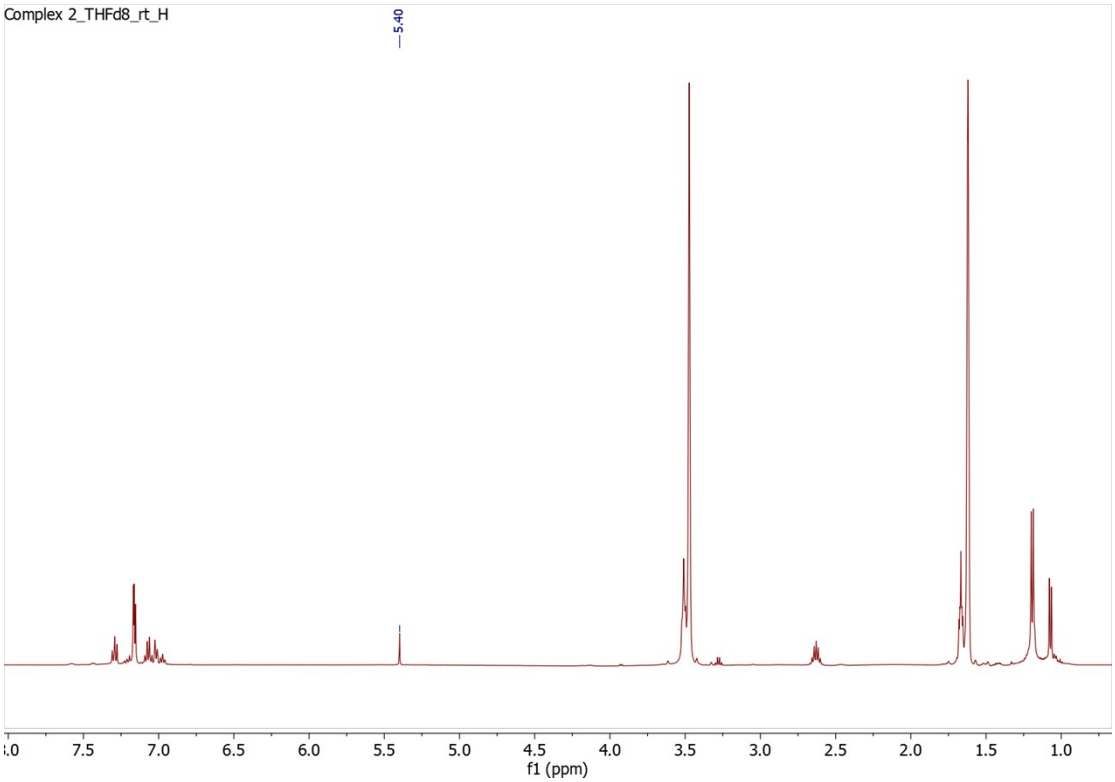

Figure S19. ^{1}H NMR spectrum of complex **2** in THF-d_8 at RT (1024 scans)

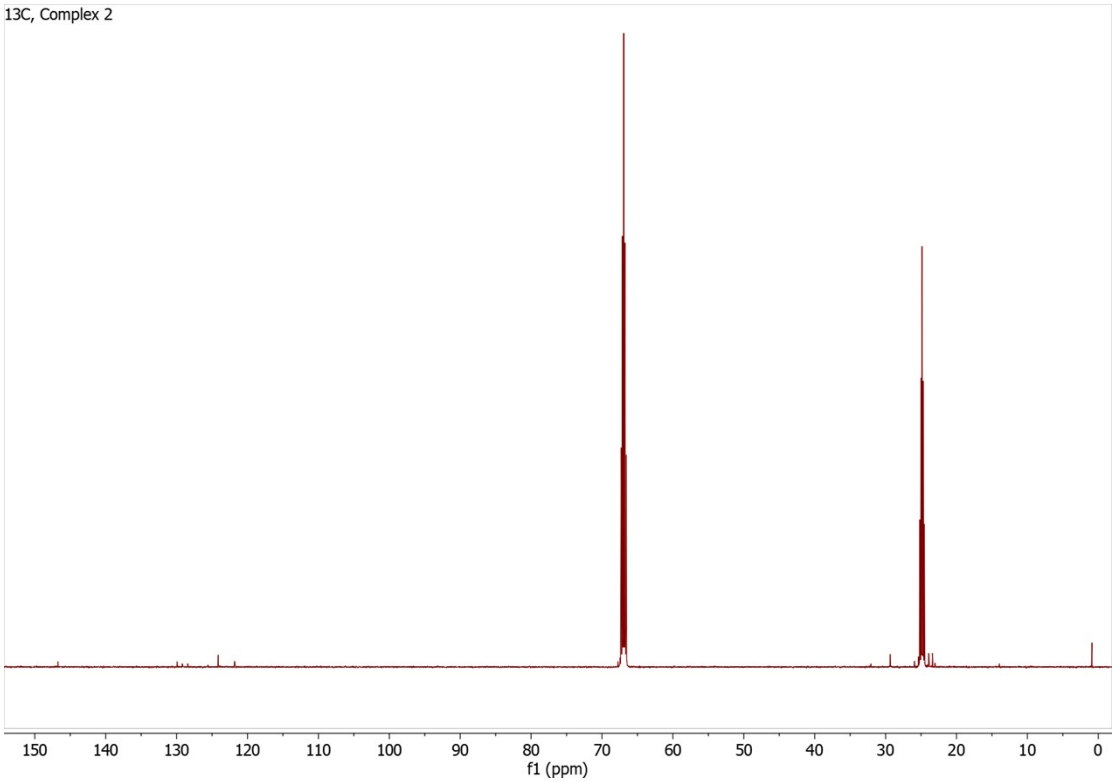

Figure S20. ^{13}C NMR spectrum of complex **2** in THF-d_8 at RT (1024 scans)

S10. Cyclic Voltammetry

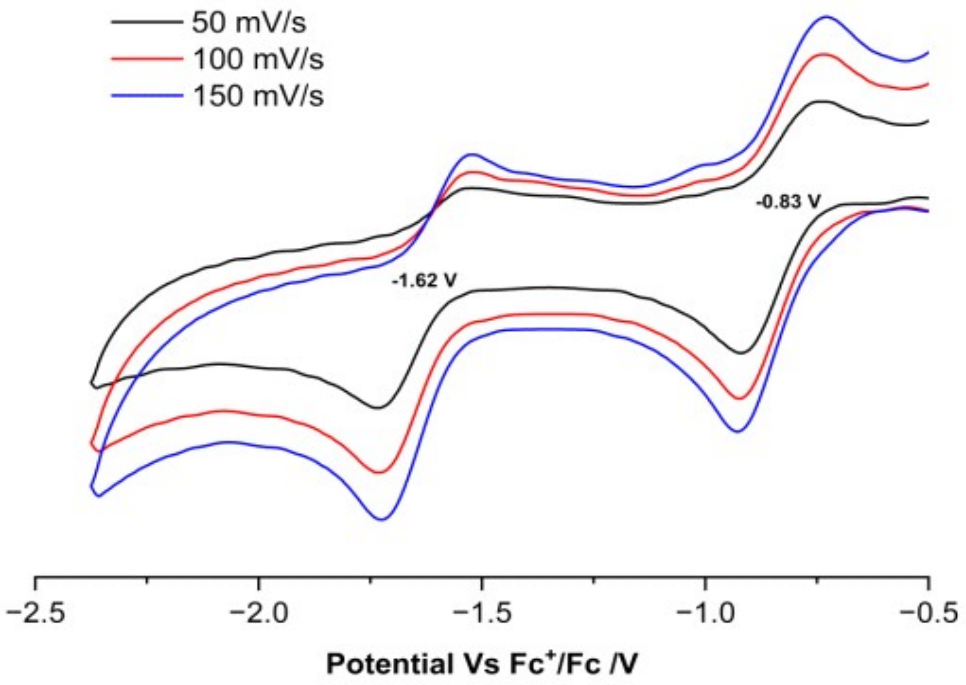

$[V^{5+}(L^{2-})_2(L^{2-})]^- \underset{e^-}{\overset{-\,e^-}{\rightleftharpoons}} [V^{5+}(L^{2-})(L^{\cdot -})] \underset{e^-}{\overset{-\,e^-}{\rightleftharpoons}} [V^{5+}(L^{2-})(L^{0})]^+$

$\Delta E_{1/2}$ = -1.62 V $\Delta E_{1/2}$ = -0.83 V

Figure S21. Cyclic voltammogram of complex **1** highlighting the redox behaviour of the ligand in THF solution of 0.1 M [*n*-Bu_4N]PF_6 with RE: Ag, WE: GC, and CE: Pt.

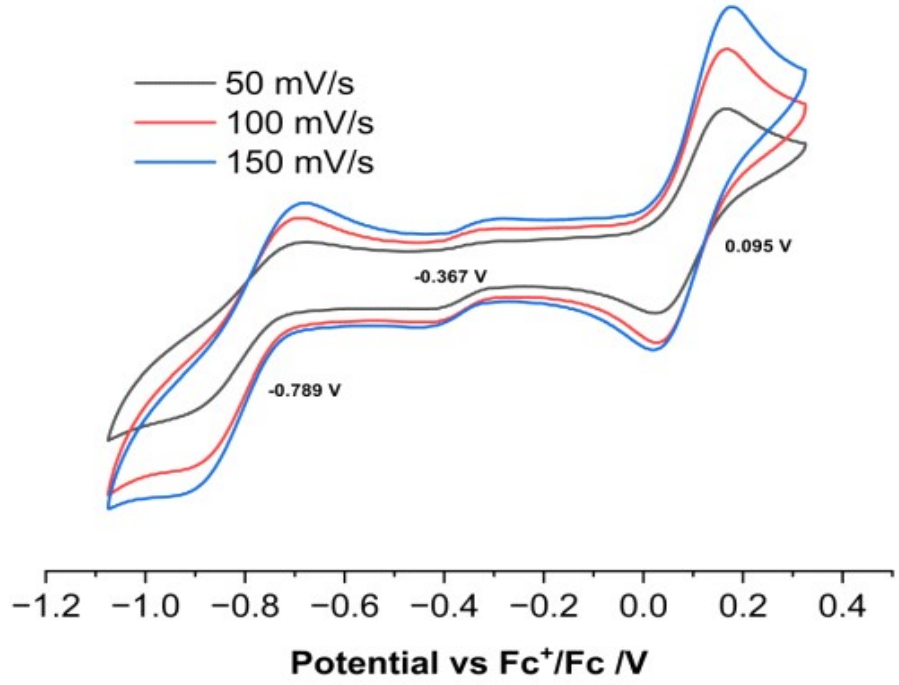

$$[V^{5+}(L^{2-})_2(L^{2-})]^{-} \underset{e^-}{\overset{-\,e^-}{\rightleftharpoons}} [V^{5+}(L^{2-})(L^{\cdot -})] \underset{e^-}{\overset{-\,e^-}{\rightleftharpoons}} [V^{5+}(L^{2-})(L^{0})]^{+}$$

$\Delta E_{1/2}$ = -0.789 V $\Delta E_{1/2}$ = -0.367V

Figure S22. Cyclic voltammogram of complex **2** in THF solution of 0.1 M [*n*-Bu_4N]PF_6 with RE: Ag, WE: GC, and CE: Pt.

S11. Electrochemical calculations

The specific capacitance was calculated through CV curves using the formula.[S20, S21]

$$C_s = \frac{\int_i^f i(V)dV}{m.\Delta V.v} \quad (2)$$

where, C_S specific capacitance (F/g), m is mass loading, ΔV is potential window and v is scan rate and integration term gives the area under CV voltammogram.

The specific capacitance, estimated through GCD curves with the help of following expression.[S21]

$$C_S = \frac{I\Delta t}{m\Delta V} \quad (3)$$

where I is applied current density, Δt is the discharge time and ΔV is potential window, m is mass loading.

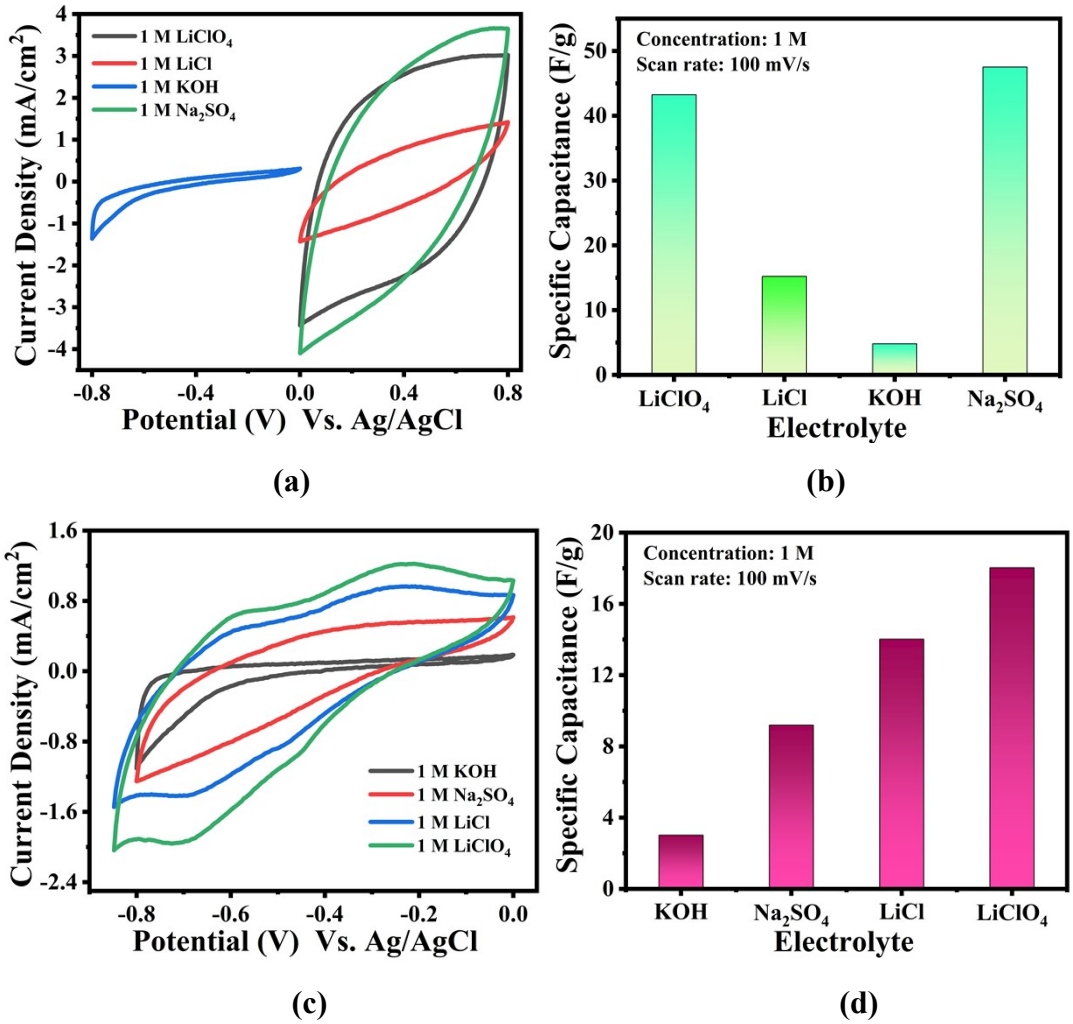

Figure S23. (a) Cyclic voltammetry of complex **1** in different electrolytes, (b) Specific capacitance of complex **1** in different electrolytes, (c) Cyclic voltammetry of complex **2** in different electrolytes, and (d) Specific capacitance of complex **2** in different electrolytes.

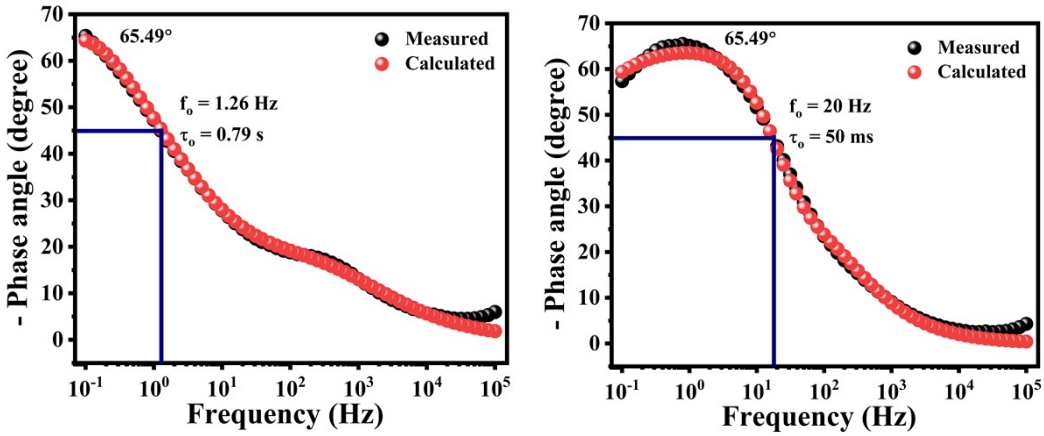

(a) **(b)**

Figure S24. Bode plots of **(a)** complex **1** and **(b)** complex **2.**

S12. EDAX Spectra

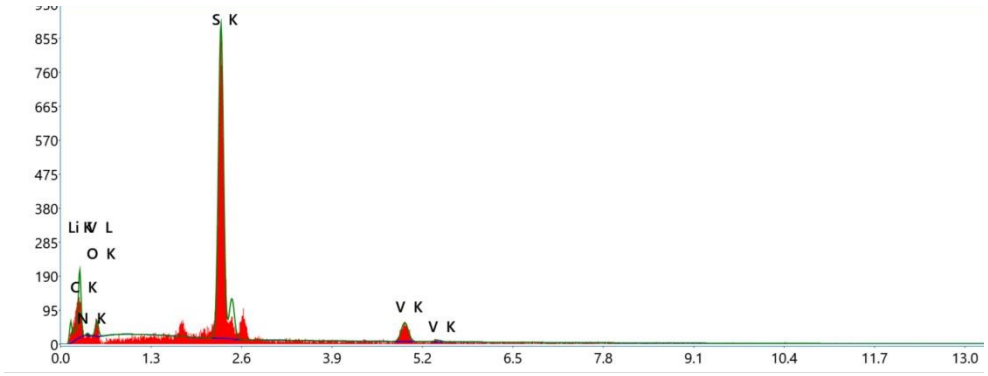

(a)

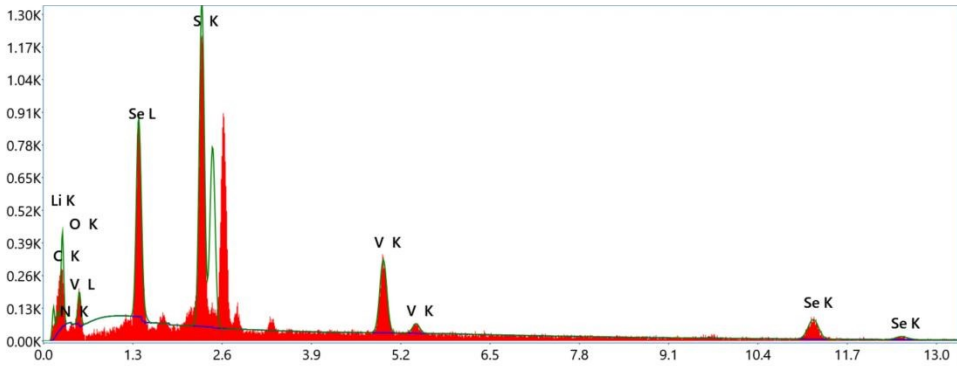

(b)

Figure S25. Energy Dispersive X-ray (EDAX) spectra of (a) complex **1** and (b) complex **2**.

S13. Raman Spectroscopy

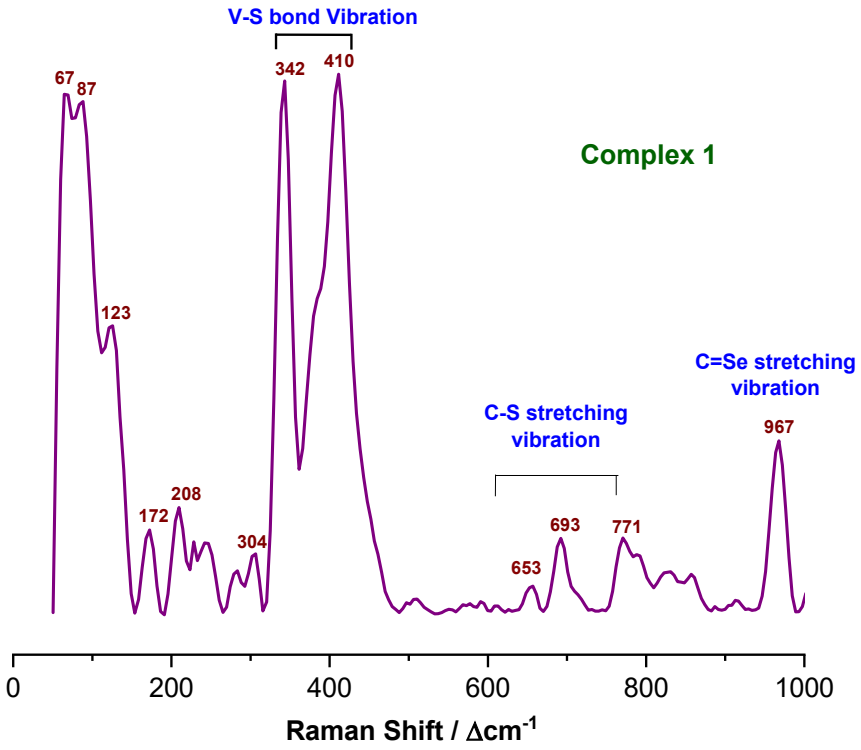

Figure S26. Solid state Raman spectrum of complex **1** measured in alpha300 R Raman Microscope.

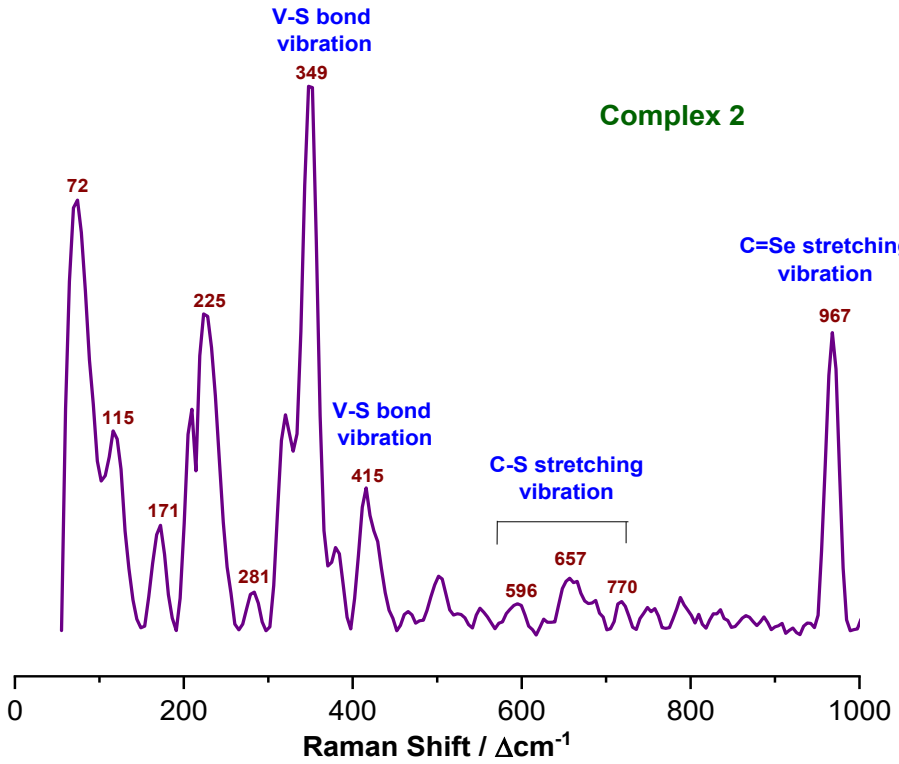

Figure S27. Solid state Raman spectrum of complex **2** measured in alpha300 R Raman Microscope.

Table S4: Assignments of bands of complexes 1 and 2

Band (cm^{-1})	Intensity	Assignment of bands	Reference range (cm^{-1})	Reference (In Manuscript)
342	Strong	V-S stretching	350	29a
410	Strong	V-S deformation	415	29a
349	Strong	V-S stretching	350	29a
415	Medium	V-S stretching	415	29a
596	Weak	C–S stretching	570-750	29b
657	Weak	C–S stretching	570–750	29b
770	Weak	C–S stretching	570–750	29b
967	Strong	C=Se stretching	995	29b

Optimized Coordinates

Complex **1a'** in BP86-D3(BJ)/Def2TZVPP, gas phase

Energy = -5440.2231883 hf

V	0.000934000	-0.001889000	0.000083000
S	6.433431000	-2.667518000	-0.000170000
S	1.376975000	-1.098089000	-1.605258000
S	-1.636699000	-0.644629000	-1.605267000
S	1.377038000	-1.097897000	1.605417000
S	0.262703000	1.737875000	-1.605272000
S	0.262572000	1.737928000	1.605285000
S	-1.636813000	-0.644593000	1.605201000
S	-5.535046000	-4.227175000	0.000055000
S	-0.903529000	6.902411000	-0.000052000
N	4.040002000	-1.876682000	1.101856000
N	4.040242000	-1.876482000	-1.101524000
N	-3.648086000	-2.555933000	1.101603000
N	-3.648204000	-2.555728000	-1.101775000
N	-0.392715000	4.434089000	1.101614000

N	-0.392389000	4.434056000	-1.101782000
C	4.840837000	-2.144433000	0.000172000
C	2.776227000	-1.458338000	-0.694298000
C	2.776173000	-1.458353000	0.694396000
C	-2.651133000	-1.673549000	-0.694391000
C	-2.651079000	-1.673635000	0.694279000
C	-4.282219000	-3.113393000	-0.000104000
C	-0.123721000	3.130160000	-0.694365000
C	-0.123850000	3.130181000	0.694324000
C	-0.560663000	5.261527000	-0.000107000
C	4.461270000	-2.018876000	-2.479062000
H	5.552242000	-2.131383000	-2.481671000
H	3.998320000	-2.905186000	-2.937481000
H	4.156647000	-1.128094000	-3.044411000
C	4.460777000	-2.018356000	2.479522000
H	3.982007000	-2.893188000	2.943586000
H	5.549572000	-2.150579000	2.480201000
H	4.174238000	-1.119046000	3.040947000
C	-3.982085000	-2.848155000	-2.479495000
H	-3.061050000	-3.056895000	-3.040068000
H	-4.647108000	-3.720326000	-2.480008000
H	-4.493645000	-1.992705000	-2.944636000
C	-3.982454000	-2.848140000	2.479248000
H	-4.639928000	-3.726001000	2.480603000
H	-3.060564000	-3.047236000	3.041840000
H	-4.502704000	-1.996379000	2.941600000
C	-0.480309000	4.869392000	2.479274000
H	-1.113379000	4.169766000	3.041234000
H	0.517066000	4.895107000	2.942393000
H	-0.913080000	5.877170000	2.480454000
C	-0.480032000	4.869133000	-2.479509000
H	0.516689000	4.888881000	-2.944270000
H	-1.118057000	4.173019000	-3.040272000
H	-0.907249000	5.879290000	-2.480195000

Complex **1b'** in BP86-D3(BJ)/Def2TZVPP, solvent phase (THF)

Energy = -5440.206745 hf

V	0.002089000	-0.001754000	0.000004000
S	-2.174695000	6.621603000	-0.000028000
S	-0.978641000	1.462126000	1.601169000
S	-0.776893000	-1.583254000	1.601287000
S	-0.978618000	1.462073000	-1.601221000
S	1.761020000	0.116940000	1.601506000
S	1.761153000	0.117012000	-1.601271000
S	-0.776520000	-1.583434000	-1.601376000
S	-4.657159000	-5.186837000	-0.000417000
S	6.826662000	-1.428661000	0.000212000
N	-1.553309000	4.178561000	-1.103465000
N	-1.552872000	4.178702000	1.103346000
N	-2.848711000	-3.430715000	-1.103478000
N	-2.848918000	-3.430523000	1.103273000
N	4.399704000	-0.745956000	-1.103154000
N	4.399588000	-0.746087000	1.103557000
C	-1.760724000	4.991075000	-0.000070000
C	-1.230674000	2.890642000	0.694768000
C	-1.230682000	2.890626000	-0.694858000
C	-1.891213000	-2.511315000	0.694651000
C	-1.890997000	-2.511477000	-0.694896000
C	-3.448982000	-4.016401000	-0.000128000
C	3.123656000	-0.379663000	0.694916000
C	3.123696000	-0.379689000	-0.694601000
C	5.207480000	-0.971980000	0.000224000
C	-1.673172000	4.600179000	2.486198000
H	-1.731388000	5.694215000	2.503437000
H	-2.580841000	4.177273000	2.940047000
H	-0.794743000	4.259557000	3.049699000
C	-1.673883000	4.599869000	-2.486340000
H	-2.579333000	4.173289000	-2.941160000

H	-1.736535000	5.693659000	-2.503253000
H	-0.793525000	4.263095000	-3.049165000
C	-3.155808000	-3.741693000	2.486419000
H	-3.291554000	-2.808629000	3.048919000
H	-4.079339000	-4.331231000	2.505209000
H	-2.340483000	-4.322839000	2.940398000
C	-3.154882000	-3.742971000	-2.486532000
H	-4.085233000	-4.321618000	-2.506723000
H	-3.277517000	-2.809970000	-3.052078000
H	-2.345180000	-4.335231000	-2.936265000
C	4.822588000	-0.855244000	-2.486493000
H	4.078368000	-1.433415000	-3.049540000
H	4.923878000	0.141834000	-2.938653000
H	5.791718000	-1.366040000	-2.506259000
C	4.822204000	-0.855794000	2.486936000
H	4.920747000	0.141084000	2.940134000
H	4.079328000	-1.436472000	3.049191000
H	5.792629000	-1.364139000	2.506447000

Complex (**1'**)$^{\bullet-}$ BP86-D3(BJ)/Def2TZVPP, gas phase

Energy =-5440.206745 hf

V	0.001509000	0.000231000	0.000065000
S	7.040297000	0.148246000	-0.000109000
S	1.751425000	-0.433125000	-1.623211000
S	-1.248763000	-1.298285000	-1.623184000
S	1.751336000	-0.432958000	1.623417000
S	-0.498140000	1.732316000	-1.623243000
S	-0.498458000	1.732332000	1.623261000
S	-1.248820000	-1.298365000	1.623262000
S	-3.394810000	-6.167125000	0.000034000
S	-3.652571000	6.017383000	-0.000214000
N	4.511345000	-0.079787000	1.095669000
N	4.511452000	-0.079527000	-1.095287000
N	-2.325265000	-3.864234000	1.095429000

N	-2.325359000	-3.864083000	-1.095538000
N	-2.187434000	3.943646000	1.095318000
N	-2.187115000	3.943686000	-1.095663000
C	5.351139000	-0.010537000	0.000196000
C	3.175500000	-0.192041000	-0.688890000
C	3.175458000	-0.192041000	0.689116000
C	-1.753193000	-2.651720000	-0.688994000
C	-1.753188000	-2.651770000	0.689004000
C	-2.686258000	-4.625536000	-0.000072000
C	-1.420322000	2.844041000	-0.689085000
C	-1.420478000	2.844034000	0.688922000
C	-2.668148000	4.635564000	-0.000217000
C	4.948041000	-0.037256000	-2.471160000
H	5.995653000	0.290256000	-2.477267000
H	4.868623000	-1.031710000	-2.937764000
H	4.309507000	0.660009000	-3.031211000
C	4.947588000	-0.037217000	2.471627000
H	4.850600000	-1.027756000	2.943040000
H	6.000464000	0.273036000	2.476081000
H	4.321272000	0.673769000	3.028371000
C	-2.507157000	-4.262827000	-2.471522000
H	-1.577176000	-4.079925000	-3.027803000
H	-2.769143000	-5.328741000	-2.475785000
H	-3.313783000	-3.680311000	-2.943543000
C	-2.507256000	-4.263098000	2.471360000
H	-2.761254000	-5.330934000	2.476305000
H	-1.579831000	-4.072249000	3.029164000
H	-3.319483000	-3.686594000	2.941233000
C	-2.443285000	4.299725000	2.471237000
H	-2.736846000	3.399612000	3.029167000
H	-1.539997000	4.719731000	2.940849000
H	-3.244937000	5.049480000	2.476349000
C	-2.442722000	4.299652000	-2.471652000
H	-1.537734000	4.714502000	-2.942518000

H	-2.741576000	3.400679000	-3.028656000
H	-3.240666000	5.053361000	-2.476422000

Complex **2a'** inBP86-D3(BJ)/Def2TZVPP, gas phase

Energy = -11450.9680374 hf

Se	-6.646536000	-2.539787000	0.000066000
Se	1.121601000	7.022538000	0.000112000
Se	5.529756000	-4.477351000	-0.000094000
V	-0.001040000	-0.001729000	-0.000355000
S	-1.400982000	-1.065645000	1.605917000
S	-0.223168000	1.742590000	1.605734000
S	-1.402157000	-1.064787000	-1.606527000
S	1.620722000	-0.681385000	1.605777000
S	-0.222065000	1.742722000	-1.606637000
S	1.620003000	-0.683305000	-1.606734000
N	-4.087394000	-1.766216000	-1.099364000
N	-4.085957000	-1.767778000	1.100608000
N	0.511857000	4.419390000	-1.100071000
N	0.510917000	4.419313000	1.099925000
N	3.574755000	-2.653220000	-1.099605000
N	3.575923000	-2.650814000	1.100348000
C	-4.886841000	-2.011336000	0.000855000
C	-2.809883000	-1.386096000	0.694509000
C	-2.810565000	-1.385409000	-0.694437000
C	0.202796000	3.123297000	0.694235000
C	0.203361000	3.123337000	-0.694754000
C	0.699768000	5.234393000	0.000029000
C	2.604675000	-1.739355000	0.694301000
C	2.604120000	-1.740516000	-0.694574000
C	4.188557000	-3.221281000	0.000573000
C	0.605378000	4.849857000	2.480304000
H	-0.395603000	5.016617000	2.904456000
H	1.113464000	4.068674000	3.060248000
H	1.169894000	5.789995000	2.501803000

C	0.607275000	4.850197000	-2.480309000
H	1.111877000	4.067103000	-3.060692000
H	-0.393230000	5.021253000	-2.903892000
H	1.175495000	5.788088000	-2.501889000
C	-4.508374000	-1.899464000	-2.479520000
H	-4.159572000	-2.853301000	-2.901691000
H	-5.604614000	-1.872601000	-2.501529000
H	-4.079352000	-1.073223000	-3.060838000
C	-4.504676000	-1.901436000	2.481357000
H	-5.601237000	-1.919378000	2.498733000
H	-4.116608000	-2.834565000	2.915188000
H	-4.113503000	-1.051545000	3.055495000
C	3.900995000	-2.945751000	2.481284000
H	2.969339000	-3.054063000	3.051723000
H	4.483834000	-3.874836000	2.496482000
H	4.496062000	-2.132054000	2.920853000
C	3.899986000	-2.950591000	-2.480029000
H	4.448667000	-3.900127000	-2.498813000
H	2.968510000	-3.019457000	-3.056608000
H	4.528815000	-2.157294000	-2.909978000

Complex 2**b'** in BP86-D3(BJ)/Def2TZVPP, solvent phase (THF)

Energy = -11451.0385626 hf

Se	2.186070000	6.773535000	-0.000511000
Se	4.792148000	-5.268376000	0.000866000
Se	-6.966746000	-1.497397000	-0.000521000
V	-0.003704000	-0.001587000	-0.000314000
S	0.052433000	1.756799000	1.602591000
S	1.491507000	-0.929831000	1.602695000
S	0.052121000	1.757242000	-1.602889000
S	-1.555251000	-0.832763000	1.601711000
S	1.491629000	-0.930437000	-1.602987000
S	-1.555671000	-0.831458000	-1.602896000
N	1.201667000	4.285476000	-1.101344000

N	1.200867000	4.285083000	1.101907000
N	3.118174000	-3.181027000	-1.101130000
N	3.117991000	-3.180537000	1.102047000
N	-4.319831000	-1.104528000	-1.101655000
N	-4.318629000	-1.107355000	1.101643000
C	1.506338000	5.053841000	0.000476000
C	0.697556000	3.054948000	0.694839000
C	0.697433000	3.055329000	-0.695127000
C	2.298495000	-2.133965000	0.695088000
C	2.298607000	-2.134234000	-0.694817000
C	3.633798000	-3.827194000	0.000649000
C	-3.002053000	-0.925836000	0.694337000
C	-3.002577000	-0.924448000	-0.695453000
C	-5.137607000	-1.226105000	0.000267000
C	3.402707000	-3.510938000	2.487750000
H	4.166386000	-2.833826000	2.895395000
H	2.479800000	-3.413402000	3.072750000
H	3.770300000	-4.542168000	2.529859000
C	3.403576000	-3.512067000	-2.486540000
H	2.481991000	-3.409893000	-3.072789000
H	4.171045000	-2.838356000	-2.892715000
H	3.766489000	-4.544952000	-2.528680000
C	1.350337000	4.696766000	-2.486825000
H	0.387555000	5.038448000	-2.891978000
H	2.075094000	5.517193000	-2.530010000
H	1.709895000	3.842384000	-3.073487000
C	1.350328000	4.693418000	2.488114000
H	2.044767000	5.539859000	2.526828000
H	0.379978000	4.996537000	2.905638000
H	1.748506000	3.850426000	3.066520000
C	-4.744801000	-1.185672000	2.488375000
H	-4.232505000	-0.404390000	3.063902000
H	-5.829060000	-1.033309000	2.525798000
H	-4.498439000	-2.170284000	2.909890000

C	-4.749130000	-1.181000000	-2.487552000
H	-5.827098000	-0.989631000	-2.527599000
H	-4.208377000	-0.424075000	-3.069275000
H	-4.539203000	-2.177632000	-2.900520000

Complex **(2')**$^{\bullet-}$ in BP86-D3(BJ)/Def2TZVPP, gas phase

Energy =-11450.9595496 hf

Se	-6.869261000	-2.134589000	0.000424000
Se	1.583975000	7.009757000	0.000315000
Se	5.295508000	-4.866209000	0.000157000
V	-0.002446000	-0.002563000	-0.000706000
S	-1.516571000	-0.977035000	1.623626000
S	-0.090370000	1.795866000	1.623119000
S	-1.518102000	-0.975920000	-1.624621000
S	1.598546000	-0.825981000	1.623217000
S	-0.088764000	1.796064000	-1.624511000
S	1.597668000	-0.828254000	-1.624619000
N	-4.247781000	-1.513939000	-1.093524000
N	-4.246262000	-1.515396000	1.094954000
N	0.810538000	4.429102000	-1.094344000
N	0.809413000	4.428962000	1.094169000
N	3.436958000	-2.915512000	-1.093889000
N	3.437938000	-2.913262000	1.094591000
C	-5.058411000	-1.712735000	0.001032000
C	-2.942631000	-1.203940000	0.689505000
C	-2.943385000	-1.203291000	-0.689464000
C	0.426583000	3.144243000	0.689128000
C	0.427269000	3.144327000	-0.689864000
C	1.044075000	5.230667000	0.000079000
C	2.511329000	-1.944834000	0.689248000
C	2.510834000	-1.945980000	-0.689707000
C	4.017728000	-3.515220000	0.000616000
C	0.932144000	4.845601000	2.473280000
H	-0.056773000	5.064750000	2.905075000

H	1.392174000	4.030119000	3.047329000
H	1.549059000	5.752945000	2.499208000
C	0.934599000	4.846022000	-2.473256000
H	1.391300000	4.028907000	-3.047617000
H	-0.053495000	5.069361000	-2.904813000
H	1.554980000	5.751000000	-2.499014000
C	-4.671289000	-1.614852000	-2.472348000
H	-4.376211000	-2.584631000	-2.902367000
H	-5.764707000	-1.524067000	-2.498671000
H	-4.187228000	-0.814337000	-3.047655000
C	-4.667465000	-1.616962000	2.474374000
H	-5.763789000	-1.570275000	2.496364000
H	-4.332161000	-2.568430000	2.915423000
H	-4.219338000	-0.790922000	3.042943000
C	3.737803000	-3.225518000	2.474120000
H	2.797315000	-3.276275000	3.039344000
H	4.268793000	-4.185893000	2.493642000
H	4.372762000	-2.444869000	2.920790000
C	3.736805000	-3.230202000	-2.472919000
H	4.234044000	-4.208367000	-2.495693000
H	2.798573000	-3.243132000	-3.043743000
H	4.403341000	-2.471032000	-2.910763000

References

[S1] G. Sun, H. Ren, Z. Shi, L. Zhang, Z. Wang, K. Zhan, Y. Yan, J. Yang and B. Zhao, *J. Colloid Interface Sci.*, 2020, **588**, 847–856.

[S2] V. U. Shankar, D. Govindarajan, R. Gopalakrishnan, T. Maiyalagan and M. J. Salethraj, *Mater. Today Commun.*, 2021, **27**, 102357.

[S3] J. Mu, J. Wang, J. Hao, P. Cao, S. Zhao, W. Zeng, B. Miao and S. Xu, *Ceram. Int.*, 2015, **41**, 12626–12632.

[S4] N. G. Prakash, M. Dhananjaya, B. P. Reddy, K. S. Ganesh, A. L. Narayana and O. M. Hussain, *Mater. Today Proc.*, 2016, **3**, 4076–4081.

[S5] V. U. Shankar, D. Govindarajan, P. Christuraj, M. J. Salethraj, F. J. Johanson and M. D. Raja, *Mater. Today Proc.*, 2020, **50**, 2675–2678.

[S6] A. Viswanathan and A. N. Shetty, *J. Energy Storage*, 2019, **27**, 101103.

[S7] K. M. Thulasi, S. T. Manikkoth, A. Paravannoor, S. Palantavida, M. Bhagiyalakshmi and B. K. Vijayan, *J. Electroanal. Chem.*, 2020, **878**, 114644.

[S8] Y. Zhang and Y. Huang, *Mater. Lett.*, 2016, **182**, 285–288.

[S9] N. Kumar, M. N. M. Ansari, S. Upadhyay, V. Gajraj, C. S, N. C. Joshi, S. Sikiru and A. Sen, *J. Mater. Chem. C*, 2023, **11**, 17022–17033.

[S10] P. H. Jampani, O. Velikokhatnyi, K. Kadakia, D. H. Hong, S. S. Damle, J. A. Poston, A. Manivannan and P. N. Kumta, *J. Mater. Chem. A*, 2015, **3**, 8413–8432.

[S11] A. Sharma, P. Mane, B. Chakraborty and C. S. Rout, *ACS Appl. Energy Mater.*, 2021, **4**, 14198–14209.

[S12] A. Qian, Y. Pang, G. Wang, Y. Hao, Y. Liu, H. Shi, C.-H. Chung, Z. Du and F. Cheng, *ACS Appl. Mater. Interfaces*, 2020, **12**, 54791–54797.

[S13]. A. D. Becke, Density-functional exchange-energy approximation with correct asymptotic behavior. *Phys. Rev. A: At. Mol. Opt. Phys.*, 1988, **38**, 3098–3100.

[S14]. S. Grimme, J. Antony, S. Ehrlich and H. Krieg, A consistent and accurate ab initio
parametrisation of density functional dispersion correction (DFT-D) for the 94 elements
H-Pu *J. Chem. Phys.,* 2010, **132**, 154104-154124.

[S15]. S. Grimme, S. Ehrlich and L. Goerigk, Effect of the damping function in dispersion
corrected density functional theory. *J. Comput. Chem.,* 2011, **32**, 1456-1465.

[S16]. F. Weigend and R. Ahlrichs, Balanced basis sets of split valence, triple zeta valence and quadruple zeta valence quality for H to Rn: Design and assessment of accuracy. *Phys. Chem. Chem. Phys.,* 2005, **7**, 3297-3305

[S17]. Gaussian 16, Revision A.03, M. J. Frisch, G. W. Trucks, H. B. Schlegel, G. E. Scuseria, M. A. Robb, J. R. Cheeseman, G. Scalmani, V. Barone, G. A. Petersson, H. Nakatsuji, X. Li, M. Caricato, A. V. Marenich, J. Bloino, B. G. Janesko, R. Gomperts, B. Mennucci, H. P. Hratchian, J. V. Ortiz, A. F. Izmaylov, J. L. Sonnenberg, D. Williams-Young, F. Ding, F. Lipparini, F. ; Egidi, J. Goings, B. Peng, A. Petrone, T. Henderson, D. ; Ranasinghe, V. G. Zakrzewski, J. Gao, N. Rega, G. Zheng, W. Liang, M. Hada, M. Ehara, K. Toyota, R. Fukuda, J. Hasegawa, M. Ishida, T. Nakajima, Y. Honda, O. Kitao, H. Nakai, T. Vreven, K. Throssell, J. A. Montgomery Jr., J. E. Peralta, F. Ogliaro, M. J. Bearpark, J. J. Heyd, E. N. Brothers, K. N. Kudin, V. N. Staroverov, T. A. Keith, R. Kobayashi, J. Normand, K. Raghavachari, A. P. Rendell, J. C. Burant, S. S. Iyengar, J. Tomasi, M. Cossi, J. M. Millam, M. Klene, C. Adamo, R. Cammi, J. W. Ochterski, R. L. Martin, K. Morokuma, O. Farkas, J. B. Foresman and D. J. Fox, Gaussian, Inc., Wallingford CT, 2016.

[S18]. E. D. Glendening, C. R. Landis and F. Weinhold. NBO 6.0: Natural bond orbital analysis program. *J. Comput. Chem.,* 2013, **34**, 1429-1437.

[S19]. A. E. Reed, L. A. Curtiss, and F. Weinhold, Intermolecular Interactions from a Natural Bond Orbital, Donor-Acceptor Viewpoint. *Chem. Rev.,* 1988, **88**, 899-926.

[S20]. B. Pandit and B. R. Sankapal, Cerium Selenide Nanopebble/Multiwalled Carbon Nanotube Composite Electrodes for Solid-State Symmetric Supercapacitors. *ACS Appl. Nano Mater.*, 2022, **5**, 3007–3017.

[S21]. S. S. Raut, J. A. Dhobale and B. R. Sankapal, SILAR deposited Bi2S3 thin film towards electrochemical supercapacitor. *Physica E Low Dimens. Syst. Nanostruct.,* 2016, **87**, 209–212.